Response of pavement foundations incorporating both geocells and expanded polystyrene (EPS) geofoam

S.M.A. Ghotbi Siabil [1], S.N. Moghaddas Tafreshi [2*], A.R. Dawson[3]

[1]*PhD Candidate, Department of Civil Engineering, K.N. Toosi University of Technology, Valiasr St., Mirdamad Cr., Tehran, Iran. Tel: +982188779473; Fax: +982188779476; E-mail address: ghotbi@mail.kntu.ac.ir*

[2,*]*Corresponding Author. Professor, Department of Civil Engineering, K.N. Toosi University of Technology, Valiasr St., Mirdamad Cr., Tehran, Iran. Tel: +982188779473; Fax: +982188779476; E-mail address: nas_moghaddas@kntu.ac.ir*

[3]*Associate Professor, Nottingham Transportation Engineering Centre, University of Nottingham, Nottingham, UK. Tel: +441159513902; Fax: +441159513909; E-mail address: andrew.dawson@nottingham.ac.uk*

Abstract: The suitability of geocell reinforcement in reducing rut depth, surface settlements and/or pavement cracks during service life of the pavements supported on expanded polystyrene (EPS) geofoam blocks is studied using a series of large-scale cyclic plate load tests plus a number of simplified numerical simulations. It was found that the improvement due to provision of geocell constantly increases as the load cycles increase. The rut depths at the pavement surface significantly decrease due to the increased lateral resistance provided by the geocell in the overlying soil layer, and this compensates the lower competency of the underlying EPS geofoam blocks. The efficiency of geocell reinforcement depends on the amplitude of applied pressure: increasing the amplitude of cyclic pressure increasingly exploits the benefits of the geocell reinforcement. During cyclic loading application, geocells can reduce settlement of the pavement surface by up to 41% compared to an unreinforced case – with even greater reduction as the load cycles increase. Employment of geocell reinforcement substantially decreases the rate of increase in the surface settlement during load repetitions. When very low density EPS geofoam (EPS 10) is used, even though accompanied with overlying reinforced soil of 600 mm thickness, the pavement is incapable of tolerating large cyclic pressures (e.g. 550 kPa). In comparison with the unreinforced case, the resilient modulus is increased by geocell reinforcement by 25%, 34% and 53% for overlying soil thicknesses of 600, 500 and 400 mm, respectively. The improvement due to geocell reinforcement was most pronounced when thinner soil layer was used. The verified three-dimensional numerical modelings assisted in further insight regarding the mechanisms involved. The improvement factors obtained in this study allow a designer to choose appropriate values for a geocell reinforced pavement foundation on EPS geofoam.

Keywords: *Geosynthetics, EPS geofoam, Geocell reinforcement, Cyclic plate load tests, Pavements*

1 Introduction

Design and construction of road embankments might involve significant challenges. Dead weight of the embankment fill generates long-term settlements in the subsoil that might require expensive pre-loading with wick drains. In extreme cases a bridge with limited soil improvement at the foundation intervals might be required. Furthermore, sourcing and movement along existing highway networks by many trucks is associated with noise, dust, emissions and congestion for a lengthy period. By introducing lightweight materials, such as EPS geofoam, the construction industry can overcome many of the mentioned difficulties and resolve further issues (some of which are addressed by Horvath, 1997; Athanasopoulos et al., 1999; Bathurst et al., 2007; Bartlett et al., 2015; El-kady et al., 2018). EPS geofoam is created by the extrusion of expanded polystyrene (EPS), constituted from numerous air-filled beads bonded together. Despite the application of EPS geofoam over the last 50 years (Khan and Meguid, 2018, Puppala et al., 2018), research on the use of EPS geofoam in construction is still ongoing, with improved guidelines and specifications being developed (Stark et al., 2004, Mohajerani et al., 2017). EPS geofoam provides a number of advantages for use as a fill material, replacing soil. These include:

a) Low density (circa 1% of soil), which reduces both dead and seismic loads,

b) Readily cut into variety of shapes,

c) Easy to install,

d) Desirable physical and mechanical properties (Horvath, 1994).

In spite of such advantages, the growth rate in this geo-technology can only be sustained where methods to enhance its use and to overcome failure are in place. With regard to the latter, early rutting (and possibly tension cracking) of overlying pavement surfaces have been observed (Horvath, 2010). This may be attributed to lack of support from the underlying EPS geofoam (Duškov, 1997a), which can result in punching of concentrated loads into the EPS geofoam due to inefficient load spreading above the EPS layer (**Fig. 1a**), as observed in the study reported later in this paper (**Fig. 1b**). This phenomenon might be due to the collapse of the foam bubbles giving it, in effect, a negative Poisson's ratio (Ossa and Romo, 2009). EPS geofoam contrasts with common soil backfills: its Young's modulus is comparable to very soft soils, its compressive strength is lower than most soils, it has different visco-elastic and visco-elasto-plastic behavior under cyclic loading (Hazarika, 2006; Trandafir et al. 2010) and it has differing stress-strain response, with a wide range of plastic strain sustained under loading (Bartlett et al., 2015, Ling et al., 2018). Furthermore, EPS geofoam is more expensive compared to soil or common low density materials, thus its consumption (in terms of bulk density) has to be minimized. By utilizing appropriate methods, e.g. as investigated in this paper, the load applied on the pavement surface may be handled such that the stress applied to EPS geofoam remains within a safe margin.

To resolve the described problems and to ensure safe performance of pavements constructed on geofoam, several techniques could be adopted. Increasing the overlying soil thickness could be a prime solution, but in some circumstances, e.g. reduction of dead and seismic loads to the adjacent retaining walls (Bathurst et al., 2007; Hazarika and Okuzono, 2004; Ertugrul and Trandafir, 2011) or distant location of the competent soil, it would be prohibitive. Using a load distribution slab (LDS) is one of the best known methods, but it requires a large amount of concrete over a significant length of the road. Moreover, it has been observed that construction of LDS overlying EPS blocks does not necessarily improve the performance of the pavement system; on the other hand, due to the higher density of concrete material compared to soil, the LDS induces overstressing of the EPS geofoam and results in failure (Horvath, 2010).

An alternative is to use soil reinforcing methods such as geocell, geogrid or geotextile (Stark et al., 2004). Geocells are three dimensional geosynthetics and a geocell mattress provides three mechanisms for increasing the load bearing capacity and improving the performance of pavement (Zhang et al., 2010; Sitharam and Hegde, 2013; Hegde, 2017): lateral resistance effect, vertical stress dispersion and membrane mechanism; thus compared to geogrids and geotextiles, geocells can deliver greater improvement due to lateral confinement and the resulting load distribution. **Fig. 1c** shows the concept: geocell has distributed settlements over a wider area with a consequent reduction in the magnitude; and this is confirmed in **Fig. 1d**. It is indicative of a wider pressure distribution compared to the punching-form of deformation (**Fig. 1b**) seen on EPS geofoam overlaid by unreinforced soil. Nevertheless, the effectiveness of soil reinforcement with geocell on EPS geofoam blocks is not studied yet. Thus, the combined use of EPS geofoam and geocell is a novel idea to resolve current shortcoming regarding highway pavements built over EPS geofoam blocks alone.

With the above description, “pavement systems supported on EPS geofoam” and “geocell reinforced pavement foundations” are the main topics that should be reviewed in this regard. Several studies have covered the use of EPS geofoam in pavements and other applications (e.g. Farnsworth et al., 2008; Kim et al., 2010; Ossa and Romo, 2012; Akay et al., 2013; Tanyu et al., 2013; Özer et al., 2014; Akay et al., 2014; Akay, 2015; Anil et al., 2015; AbdelSalam and Azzam, 2016; De et al., 2016; Keller, 2016; Liyanapathirana and Ekanayake, 2016; Ni et al., 2016; Witthoeft and Kim, 2016; Özer, 2016; Beju and Mandal, 2017; Meguid et al., 2017a,b; Gao et al., 2017a,b; Shafikhani et al., 2017; Pu et al., 2018; Selvakumar and Soundara, 2019; AbdelSalam et al., 2019; Abdollahi et al., 2019) but none of these consider the possible use of geocell reinforcement.

Likewise, a number of researchers have studied the influence of geocells on the settlements and load distributions in footings, pavement systems, etc. (Wesseloo et al., 2009; Zhang et al., 2010; Thakur et al., 2012; Tavakoli Mehrjardi et al.; 2012; Biswas et al., 2013; Chen et al., 2013; Leshchinsky and Ling, 2013a; Hegde and Sitharam, 2015a; b; c; Biabani et al., 2016a; b; Ngo et al., 2016; Suku et al., 2016; Abu-Farsakh et al., 2016; Vahedifard et al., 2016; Hegde and Sitharam, 2017; Hegde, 2017; Dash and Choudhary, 2018; Moghaddas Tafreshi et al. 2018; Ouria and Mahmoudi, 2018; Pokharel et al., 2018; Rahimi et al., 2018a; b; Satyal et al., 2018; Tavakoli Mehrjardi and Motarjemi, 2018; Venkateswarlu et al., 2018; Choudhary et al, 2019; Liu et al., 2019; Song et al., 2018;2019; Punetha et al., 2019, Neto, 2019; Tavakoli Mehrjardi et al., 2019; Fazeli Dehkordi et al., 2019). The underlying bed used in these studies can be conveniently divided into "competent ground" and "soft ground". EPS blocks would normally be employed to reduce the pressure on soft subsoils, while EPS geofoam itself can be considered as a weak support (comparable to "soft ground") to its overlying layer. So the purpose of geocell mattresses would then be to distribute the applied pressure over a larger area to prevent extensive damage or failure of the EPS and also in the subsoil below the loaded area. However the possible extent of usage and effectiveness of such method (geocell) for pavements with EPS geofoam as the underlying base material needs further investigation.

In one study, Zou et al. (2000) performed cyclic loading tests on EPS geofoam supported pavements in a special model facility. They concluded that even though the permanent deformation during load cycles is similar to sand pavement, the higher resilient deformations caused by the underlying EPS significantly increases depth of surface ruts. Thus such deformations must be limited by some means. On the other hand, Satyal et al. (2018) used large scale tests and 3D finite element analyses to study the improved performance of geocell on soft subgrades. They concluded that geocell reinforcement had the greatest efficacy in reducing settlement on weak subgrades and it also helped to reduce the rate of continuous settlement due to cyclic loading. Similar to this study (in terms of material and overall configuration) but different in the purpose, Tanyu et al. (2013) performed large-scale cyclic loading tests on geocell-reinforced gravel subbase over a weak subgrade. EPS blocks were used to simulate a soft clay bed and the soil layer was compacted lower than typical values (at ~90% of standard proctor test). They concluded that geocell reinforcement causes a 30-50% reduction in the plastic deformation of the pavement surface and improves the resilient modulus of the pavement by 40-50%.

Above all, Hegde (2017) brought a comprehensive summary on the ongoing and past research of geocell that revealed considerable facts. Based on his study, the majority of past research on geocells has been restricted to static tests in small scale, which are probably affected by scale effects. They also reported that further 3D numerical modeling is needed to comprehend the effect of geocells on pressure redistribution and surface settlements. As a conclusion, studies that combine the use of geocell reinforced soil layer and EPS geofoam blocks are still rare. Although the geocell mattress placed above an EPS layer might be considered to behave in a similar manner to the same geocell layer placed on soft soil, prediction of the overall behavior of such system would be complicated due to the variety observed in the properties of the participating elements (e.g. soil, EPS geofoam and geocell). This complexity becomes more evident when it is reminded that the behavior of EPS geofoam is dissimilar to soil under the repeated loading of traffic (Trandafir and Erickson, 2011).

This brief review of previous research indicates the effectiveness of geocell when placed over soil beds in various conditions. Geocell might, therefore, be suitable for beds formed of EPS geofoam blocks in backfill construction (Stark et al., 2004) – so the study reported in this paper was performed with the aim of investigating this possibility and the effect of contributing factors. Various methods have been used for investigation of pavement foundations subjected to repetitive loading. A great number of these studies have implemented well-known evaluation methods, such as plate load test, yet there has been several efforts for introducing novel methods or materials into application (Gnanendran et al. 2011; Piratheepan et al. 2012; Arulrajah et al. 2012; Arulrajah et al. 2013; Arulrajah et al. 2014; Rahman et al. 2015; Jegatheesan and Gnanendran, 2015; Donrak et al. 2016; Arulrajah et al. 2017; Georgees et al. 2018; Tavira et al. 2018). For instance, Piratheepan et al. (2012) combined Indirect Diametral Tensile (IDT) and Unconfined Compressive Strength (UCS) tests to estimate cohesion and internal friction angle of conventional granular material stabilized with slag lime and general blend (GB) cement-fly ash. Tavira et al. (2018) used plate load and falling weight deflectometer tests to characterize construction and demolition waste (CDW) used as base and subbase materials. Yet, the plate load test still remains a simple and practical method for evaluation of pavement foundation systems, and was also used in this study. Overview of the research aims and properties of the material used in this study are addressed in the following sections.

2 Objectives

With the above background, it would be worthwhile to characterize the effectiveness of geocell reinforcement on improving the performance of pavement foundation supported on EPS geofoam blocks. Considering previous research and preliminary evaluations prior to main tests, several parameters (e.g. reinforced and unreinforced soil thickness, EPS density) were found out to be the key influencing factors that need further investigation. Based on these factors, the main objectives of this study are:

- To study the effectiveness of unreinforced and geocell reinforced overlying soil layers in the distribution of load onto an underlying EPS geofoam layer,
- To compare the surface settlements of unreinforced and geocell reinforced EPS pavements,
- To determine the simultaneous effect of soil thickness and geocell reinforcement on the behavior of pavement foundations resting on EPS geofoam,
- To determine whether thinner soil layers over EPS geofoam are practical when geocell reinforcement is used in the soil layer, and,
- To describe the effect of EPS densities on the performance of EPS pavements overlaid by geocell reinforced soil.

To achieve these, a series of full-scale repeated plate load tests were conducted. In addition to the experimental tests, a shortened Finite Element analysis was used to assist with better understanding of mechanisms, and interpretation of experimental results.

3 Material characteristics

The soil, EPS geofoam and geotextile used in this study was previously used by Ghotbi Siabil et al. (2019). A brief description of the material characteristics is given here.

3.1 Soil

The specifications of ASTM D 2940-09 were employed to classify the soil according to the requirements of highway and airport pavements. According to the Unified Soil Classification System (ASTM D 2487-11), the soil is well-graded sand (SW) (see **Fig. 2**) with specific gravity (G_s) of 2.66. Maximum and mean grain size of the soil were 20 and 4.3 mm, respectively. Using the modified proctor compaction test (ASTM D 1557-12), the peak dry density of soil was obtained as 20.42 kN/m^3 at 5% optimum moisture content. Triaxial compression tests on the soil with 5% moisture content and dry unit weight of 19.72 kN/m^3 (97% of the modified Proctor maximum density) showed an internal friction angle of 40.5º. Additional information regarding soil particle size and grading parameters are shown on **Fig. 2**.

3.2 EPS geofoam

The original size of EPS geofoam blocks produced by the molder was 1000×1000×2000 mm. The blocks were cut into the desired dimension (1000×500×200 mm or 1000×500×100 mm) by using a hot wire. Measurement of EPS density was performed according to ASTM D 1622-08 and the remaining properties were in accordance with ASTM D 7180-05. To obtain the compressive strength, elastic modulus and resilient modulus of the EPS geofoam, static and cyclic uniaxial compression tests were performed on 200 mm cubic specimens (the section area of the samples satisfy recommendations of ASTM D 1621-00 by far). Negussey (2007) reported that the physical properties obtained from testing larger EPS geofoam samples are more accurate compared to smaller ones. The resilient moduli were obtained under the maximum cyclic pressures, for which the EPS strained in a stabilizing manner (see P_s in **Table 1**, derived from Ghotbi Siabil et al., 2019). The frequency of EPS sample tests (and cyclic plate load tests on the EPS geofoam pavement system) was selected 0.1 Hz to obtain a lower bound for the cyclic stress that generates permanent deformation in EPS geofoam (Trandafir et al., 2010). According to Trandafir et al. (2010), cyclic axial strain up to 0.87-1.0% can be considered as the critical cyclic strain value, beyond which plastic yielding and permanent plastic strains occur in EPS geofoam. In agreement with these studies, the stable threshold of cyclic pressure (P_s) can be defined as the cyclic stress that can be applied 100 times over the full face of a 200 mm EPS geofoam cube, with the cube averagely sustain 0.05% normal strain per cycle – a stable plastic shake-down is observed at such condition (Collins and Boulbibane, 2000; Yang, 2010). The shear strength parameters of EPS geofoam (expressed as cohesion and angle of internal friction) were obtained from unconsolidated undrained triaxial compression testing under confining pressure of 50, 100 and 150 kPa on cylindrical specimens of EPS geofoam with diameter and height of 100 mm 200 mm, respectively. The axial loads in these tests were applied at a constant strain rate of 1.5 mm/min (ASTM D2850-15). The summary of the properties for EPS with densities of 10, 20 and 30 kg/m^3 is presented in **Table 1** from which it will be seen that the EPS is, essentially, non-frictional – possessing only cohesive strength.

3.3 Geocell reinforcement

The geocell employed in this study was formed from nonwoven geotextile comprising continuous polypropylene strands, thermo-welded under pressure ("melded") at regularly spaced points so that, when the strands are pulled apart a 'honeycomb' arrangement is formed (see Fig. 4b). Thus the strength of the geocell joints is generally similar to its base fabric material. The soil is transferred into the cells and then compacted to produce a composite mattress with enhanced properties (increased apparent cohesion and higher stiffness). This improvement is attained by confining the soil by passive resistance and limiting its lateral spread (Thakur et al., 2012). Consequently, the geocell reinforced soil composite provides higher load-bearing capacity and improved performance under cyclic loading. The height and average diameter of geocell pockets were 100 and 110 mm, respectively. The engineering properties of the geocell base material (geotextile) were kept constant in the tests and the values are provided in **Table 1**.

3.4 Geotextile separation

According to previous recommendations (e.g. Stark et al., 2004), the EPS geofoam should be insulated from direct contact with the overlying soil layer by means of a geotextile layer to prevent possible damage to the EPS geofoam. For this purpose, a non-woven geotextile with the properties reported in **Error! Reference source not found.** was used. This geotextile is made of UV-stabilized polypropylene and is needle-punched, heat bonded and is recommended for separation, filtration, reinforcement and protection in building and construction applications.

4 Description of experiments

4.1 Test box and simulated loading

In this study, repeated plate load testing was employed to mimic the loading applied by a truck tire as recommended by AASHTO T 221-90 and ASTM D 1195-09 for soils and flexible pavement components. For this aim, the model pavement sections were constructed in a test box of 2200×2200 mm in plan and 1200 mm (could be increase up to 1400 mm) in depth. The interior sides and bottom of the box were covered with a rough layer of cement-sand mixture and unreinforced concrete, respectively. In agreement with the observations that will be described in **Fig. 6** and **Section 6**, the box dimensions fulfilled the recommended values by Thakur et al. (2012) – a horizontal dimension of 7 times of the loading plate (which would be 2100 mm in this study) – and by Moghaddas Tafreshi et al. (2014) who indicated that a 700 mm deep test box would be sufficient to prevent possible stress redistribution induced from bottom of the box (box depth is ≥1200 mm in this study). Along with the above suggestion, DeMerchant et al., (2002) used a 305 mm plate in a 2200 mm width and 860 mm deep test box for studying geogrid-reinforced lightweight material and confirmed that the results were not altered by the side or bottom boundaries. Accordingly, Hegde and Sitharam (2015b) found that the pressure dispersion depth (where pressure is ≤10% of the bearing capacity) would be 1.6B and 1B for an unreinforced and a geocell-reinforced soft clay bed, equivalent to 480 mm and 300 mm in this study. Thus the dimensions of the test box employed here are more than sufficient on the basis of previous researchers' results and rationales.

To simulate the repetitive pressure induced from light and heavy trucks, a loading device consisting of a rigid frame, cyclic load actuator, piston, load cell and 300mm diameter/25mm thick rigid loading plate (repetitive plate load testing is recommended by AASHTO T 221-90 and ASTM D 1195-09 for soils and flexible pavement components) and other equipment were incorporated (**Fig. 3a**). Brito et al. (2009) proposed that amplitudes 400 kPa and 800 kPa can be representative of half- and fully-loaded trucks. At least a thin asphalt layer is employed at the top of pavements, which was not replicated in these tests. Thus the recommended pressures were reduced to 275 kPa and 550 kPa on the basis of calculations made using the KENPAVE software (Huang, 1993).

ASTM D 1195-09 suggests the use of static plate loading, with a few load repetitions, on soils and unbound base and subbase materials for evaluation and design of highway and airport flexible pavements. Although the number of vehicle passes will definitely exceed these values by a large margin, the pressure on the unbound layers will be greatest, and most critical, in the construction phase of the road, when the covering materials are at their thinnest (or even absent). At such a stage, Powell et al (1984) showed that 500 axle passages is a likely maximum. Thakur et al. (2016) only applied 100 cycles of 550 kPa pressure to evaluate deformation of geocell-reinforced recycled asphalt pavement bases subjected to repetitive loading. Similarly Sun et al. (2015) who applied 100 cycles of pressure at various loading increments up to 700 kPa to investigate the performance of geogrid-stabilized unpaved roads under cyclic loading. From the above background, the present authors adopted two loading stages:

(1) A first stage of loading comprising 100 applications at 275 kPa, which is followed by

(2) A second stage with 400 repetitions of 550 kPa pressure (**Fig. 3b**).

The cyclic pressure was applied in sinusoidal form with 0.1 Hz frequency, approximately the median of the frequencies adopted by Palmeira and Antunes (2010), Yang et al. (2012), Thakur et al. (2012) and Gonzalez-Torre et al. (2015).

4.2 Measurement system

Various data acquisition sensors were required to record data and permit loading control. A 100 kN load cell of S-shape with accuracy of ±0.01% was utilized to regulate the intensity and rate of loading. To measure the settlement of loading surface, two LVDTs were placed above and touching the loading plate. In some of the tests, additional LVDTs were used at distances of 250 mm, 400 mm and 600 mm from the center of the loading plate so as to permit generation of a surface settlement profile (see **Fig. 3a**). The LVDTs had a full range of 75 mm with an accuracy of ±0.01%. A pressure cell of 1 MPa capacity was placed on top of EPS layer in all of the tests to measure the pressure transferred to the top of the EPS geofoam layers (P_t), at the position where the pressure intensity would be critical to the overall response of the pavement system. All of these instruments (indicated in **Fig. 3a**) were connected to a data logger which processed and passed the data to a computer for future use.

4.3 Backfill preparation and test procedure

EPS geofoam blocks (1000 × 500 mm in plan and 200 mm thickness) were placed at the bottom of the test box. The blocks must be placed in tight arrangement together, to prevent increased settlements originating from gaps between the EPS blocks (Zou et al, 2000 and Duškov, 1997b). The blocks were leveled properly and differential surface alignments were minimized. For placing the subsequent layers of EPS geofoam, the direction of the longest side of the blocks was aligned perpendicular to those of the underlying blocks, so as to form an integrated mass of EPS, and minimize relative vertical displacement of the blocks (Stark et al., 2004). No connection or adhesive was used between EPS geofoam blocks due to expensiveness for practical applications. **Fig. 4a** displays the test box after preparing the EPS bed.

After completion of the placement of EPS geofoam layers, a geotextile sheet with 16 kN/m strength (see **Error! Reference source not found.** for the properties of geotextile) was placed over EPS bed to separate it from soil, as recommended by Stark et al. (2004). The importance of the covering geotextile is due to the soft texture of EPS geofoam, which is sensitive to damage when directly in touch with any soil that has a rough nature. Then, the soil was transferred into the test box by means of hand shovels, spread and leveled to reach a pre-determined thickness. This pre-compaction thickness was determined, by trial and error, to be approximately 120 mm for unreinforced pavements. A 450 mm wide walk-behind vibrating compactor was used across to compact the soil until it reached the desirable thickness of 100 mm for unreinforced pavements. Therefore, for each unreinforced soil thickness of 400, 500 or 600 mm, the soil layer was compacted in 4, 5 or 6 layers, respectively. **Fig. 4b** shows the typical placement of geocell in the test box.

According to Moghaddas Tafreshi et al. (2014), the optimum installation depth of geocell (u) is 0.2 times the diameter of the loading plate (u/D = 0.2). Hence, with a loading plate diameter of 300 mm in this study, the optimum depth of geocell mattress becomes u = 60 mm. For this reason, the final compacted layer above the geocell and the geocell layer itself had thicknesses of 60 and 100 mm, respectively. Thus, for reinforced pavements with total soil thicknesses of 400, 500 and 600 mm, the remaining thickness of soil below geocell mattress would be 240, 340 and 440 mm, which were divided, nominally, into 2×120, 3×113 and 4×110 mm layers, respectively. The width of geocell mattress was selected as approximately 5 times the diameter of loading plate in accordance with Thakur et al., 2012 and Moghaddas Tafreshi et al. 2014.

Regular in-situ measurements of density according to ASTM D1556-07 showed that the degrees of compaction achieved were almost equal for both unreinforced and reinforced pavements at the same depth. The maximum obtainable density was found to be a function of the height of soil placed above the EPS geofoam and reinforcement status of the soil layer. The first layer of soil placed directly on the EPS geofoam could be compacted up to 91.5% of the modified Proctor maximum (a dry density of 18.7 kN/m^3), while the second, third and fourth layers achieved 93.5%, 95% and 96% (equivalent to dry densities of 19.1, 19.4 and 19.6 kN/m^3), respectively. For the fifth and sixth layers of soil, when needed, dry densities higher than 19.6 kN/m^3 were almost unreachable. However, inside the geocell the density could be expected approximately 2-4% lower in the unreinforced soil (Moghaddas Tafreshi et al., 2014). The difference can be explained in terms of the geocell wall friction and multiple geotextile boundaries against which uninterrupted packing becomes impossible. In **Fig. 4c**, the final instrumented model pavement is presented.

5 Test program and parameters

According to the previous studies (Ghotbi Siabil et al., 2019) and preliminary numerical analysis in the current study, the compacted soil thickness (h_s), density of the upper EPS layer (γ_{gt}) and density of the bottom EPS layers (γ_{gb}) are the factors having the most significant effect on the response of these pavements (see **Fig. 3a** for definition of parameters) - the subscripts “s”, “g”, “t” and “b” stand for soil, geofoam, top and bottom, respectively. For simple representation, the density of the upper and bottom EPS layers are shown as “EPS γ_{gt}/γ_{gb}” in this paper. The thickness of the upper and bottom EPS layers (h_{gt} and h_{gb}, respectively) are also influencing factors. When the thickness of the overlying stiffer EPS (e.g. in EPS 30/20) is less than 200 mm, the upper EPS block would rupture due to excessive bending tension in EPS under higher applied pressures (Ghotbi Siabil et al., 2019). Thus, in all tests, the thicknesses of the upper EPS and bottom EPS layers were selected 200 mm and 600 mm (h_{gt} = 200 mm and h_{gb} = 600 mm), respectively. The thickness of the EPS block sheets was selected as 200 mm in these tests. With a total 800 mm thickness of EPS geofoam bed in this study, the number of EPS layers is four (greater than the minimum two recommended by Stark et al., 2004).

Gandahl (1988) and PRA (1992) had proposed using a minimum of 300-400 mm thickness for the overlying soil layer, while Stark et al. (2004) has suggested increasing it to 610 mm. A great advantage of geocell reinforcement would be to decrease thickness of the overlying soil layer, consequently reducing construction duration and costs. As previously stated, one of the objectives of this study is to characterize pavement foundations overlaid by thinner soil (i.e. 400 and 500 mm) that contains a geocell layer. Therefore, the thicknesses of the overlying soil layer used in this study is (almost) in accordance with Stark et al. (2004), Gandahl (1988) and PRA (1992), varying from 400 to 600 mm.

The Test Series as shown in **Table 3** was designed to study the effects of the above-mentioned factors. Test Series 1 was performed to provide an understanding on the pressure distribution in the subsequent layers of reinforced and unreinforced pavement foundations. Test Series 2 was performed to evaluate the effect of geocell reinforcement (used at different thicknesses of the overlying soil layer) on the performance of the pavement foundation. By comparing the results of Test Series 2, the remaining Test Series (i.e. Test Series 3, 4 and 5) were performed so as to discover the effect of reducing the density of EPS layers and decreasing soil thickness on the reinforced and unreinforced pavements' response. In order to ensure the repeatability of the tests, each Test Series was repeated a few times. This showed that a close match existed between test results, with a variation not greater that 7%. Mean results are discussed hereafter.

6 Experimental results

For easier comparison of test results, two improvement factors (*IF*) are introduced:

$$IF\delta_{m.n} = \frac{\delta_{\mathrm{u.m.n}} - \delta_{\mathrm{r.m.n}}}{\delta_{\mathrm{u.m.n}}} \times 100 \quad \textbf{(1)}$$

$$IFp_{\,m.n} = \left(\frac{p_{\mathrm{u.m.n}} - p_{\mathrm{r.m.n}}}{P_s}\right) \times 100 \quad \textbf{(2)}$$

$\boldsymbol{\delta_{X.m.n}}$: *Total or residual (permanent) surface settlement (mm)*

$\boldsymbol{p_{X.m.n}}$: *Vertical stress at point of interest, e.g. on EPS geofoam (kPa)*

X*: Reinforcement status (**r** for reinforced and **u** for unreinforced)*

$\boldsymbol{P_s}$: *Stable pressure threshold for each EPS density from Table 1*

n*: Number of load cycles, the cycle number is reset to 1 for the first cycle of the second stage*

m*: 1 and 2 for the first and second loading stages (pressures of 275 and 550 kPa applied to loading plate, respectively)*

In **Eq. 1,** $IF\delta$, is an improvement factor to compare the *total or residual (permanent) surface* settlements of the reinforced and unreinforced beds, normalized to the unreinforced surface settlement and in **Eq. 2**, and *IFp* is used to compare the pressures in the two beds, normalized to the stable pressure threshold (P_s from **Table 1**). To obtain a realistic insight regarding settlement changes in the second loading stage, the final (or last cycle) residual settlement in the first loading stage ($\delta_{X,1,100}$) was subtracted from the total (accumulated) settlements at the end of the second loading stage ($\Delta_{X,2,n}$) so as to represent net values which are also presented in the summary tables. The following equation describes this:

$$\delta_{X.2.n} = \Delta_{X.2.n} - \delta_{X.1.100} \quad \textbf{(3)}$$

Where the subscripts are as for **Eq.s 1** and **2**.

From Eq. 1, $IF\delta_{2,400}$ describes the proportional reduction (or enhancement) in surface settlements of reinforced pavement foundation compared to unreinforced one, under 550 kPa loading after 500 total cycles (i.e. cycles 1 – 400 under the higher loading). Also from Eq. 2, $IFp_{2.400}$ describes the proportional reduction (or enhancement) in the pressure transferred to EPS geofoam in the reinforced pavement foundation compared to unreinforced one to the stable stress threshold at any selected depth, under a 550 kPa surface loading after 500 total cycles (i.e. cycles 1 – 400 under that higher loading). Positive IF values indicate improvement (i.e. reduction in settlement or pressure of reinforced foundation compared to unreinforced one) and negative IF values (enhancement in settlement or pressure of reinforced foundation compared to unreinforced one) indicate insufficiency in density of the underlying EPS geofoam, despite geocell-reinforcement.

In any individual loading cycle, as the stress is applied through the loading plate, the surface settlement increases from a minimum value to a peak value. Then, during unloading, due to the elasto-plastic nature of the soil and EPS geofoam, only the elastic part of the settlement is recovered, but the plastic component remains. In other words, surface settlement increases from a minimum value to a maximum ("peak") value during each loading cycle before returning to a new minimum ("residual") value which is slightly larger than the previous minimum. It is clear that both the peak and residual settlements increase with load cycle number. Both are important, therefore the envelope formed by the peak and residual surface settlements have been plotted in Fig. 5b while examples of the extracted peak and residual (permanent) curves are shown in **Fig. 7a, b** and **10a, b**.

6.1 Overall pavement responses

First, it would be beneficial to provide a typical comparison of reinforced and unreinforced pavement foundations in terms of surface settlement and transferred pressure on EPS geofoam in **Fig. 5a** to **Fig. 5d**. For the installation reported in this plot, thickness of the overlying soil layer is 400 mm and density of the top and bottom EPS layers are 30 and 20 kg/m^3, respectively (Test Series **2a** and **2d**). During the first stage of loading (275 kPa applied pressure), variation of surface settlements for the unreinforced and reinforced cases is analogous each other, both reaching to about 5 mm after 100 load repetitions. To show the precise pressure-settlement path, **Fig. 5a** was magnified for the first ten load cycles and is shown separately in the bottom-right corner of the figure. As is commonly seen in repeated loading results, the first cycle of loading shows an atypically larger amount of settlement, probably due to bedding effects. Distinguishingly, the second stage of loading (550 kPa applied pressure) involves progressively increasing settlement increments during loading repetitions for the unreinforced case. Thus the development of accumulated permanent and resilient deformations is evidently larger compared to the reinforced case. It is inferable that the reinforced case demonstrates stable shakedown state, while the unreinforced one shows an unstable shakedown (Thakur, 2013) and might end up in failure due to incremental collapse after more load repetitions (Yang, 2010). The final (of last cycle) peak surface settlement of the unreinforced and reinforced pavement foundations reach to 25.08 and 16.53 mm, respectively – indicating a notable reduction (34%) in surface settlement due to geocell provision.

Diagrams of the pressure transferred to EPS geofoam (P_t) can assist in explaining the described observations (see **Fig. 5c** and **Fig. 5d**). During the first loading stage, the peak value of P_t in unreinforced and reinforced cases remains averagely around 36 and 30 kPa, respectively. These pressures are substantially lower than the stabilizing pressure threshold of EPS 30 (P_s = 140 kPa as given in **Table 1**). With increasing the applied pressure to 550 kPa in the unreinforced case, the pressure transferred to EPS geofoam exceeds 120 kPa in the first cycle and gradually rises up to about 140 kPa, which is identical the critical threshold stress for EPS 30 – a failure is expected beyond this point. However, P_t remains below 100 kPa (significantly lower than P_s for EPS 30) for the reinforced case during this stage. The rate of change in P_t is increasing for the unreinforced case and slightly decreasing for the reinforced case, representing progressive failure of soil due to strain accumulation (**Fig. 5a**) and shakedown states (**Fig. 5b**), respectively. Similar performance improvement due to provision of geocell in subballast was also reported by Indraratna et al. (2015). Thus the reinforcement acts to reduce the stress to tolerable levels, thereby preventing strain accumulation in soil due to accumulative irrecoverable strain/damage in the underlying EPS geofoam.

Lateral resistance of the geocell walls prevents soil from early shear failure and also provides significant confinement which prevents initiation of failure surfaces. Hegde and Sitharam (2015b) observed when the underlying bed is weak, geocell can resist the foundation load even after failure of the weak bed. It is reported that large repeated stress applications cause progressive punching in a thinner unreinforced soil layer lying over EPS due to the weak support (Duškov, 1997b) and/or low (or even negative) Poisson's ratio of the underlying EPS geofoam (Ossa and Romo, 2009; Trandafir et al. 2010). Thus it can be concluded that in a geocell-reinforced soil layer placed over an EPS geofoam bed, "vertical stress dispersion" mechanism could be the prime resistance against lower applied pressure. When the pressure is increased and the EPS layer subsequently deforms excessively below the pressurized zone, "lateral resistance" and "membrane mechanisms" would be effective. However, studies are required to confirm these predictions.

6.2 Transferred pressure in EPS layers

The performance of EPS geofoam pavement foundations appears to be sensitive to the level of stress that is asked to bear. Therefore, the results of Test Series 1 were reviewed (see **Table 3**) to determine the pressure transferred to the EPS layers and to assess the effect of geocell reinforcement. The thicknesses of soil, upper EPS and bottom EPS layers were 400, 200 and 600 mm, respectively. The density of upper and bottom EPS layers (γ_{gt} and γ_{gb}) were 30 kg/m^3 and 20 kg/m^3 (EPS 30/20), respectively. The pressure transferred at five depths, i.e. 400 mm (interface of soil layer and top of EPS layers), 600, 800, 1000 and 1200 mm from the backfill surface (at interface of soil and EPS block layers), were measured by placing a pressure cell at that specific depth – i.e. in five similar tests with various embedment depth of pressure cell (see **Fig. 3a**).

Fig. 6a and **6b** display the peak vertical pressure in the EPS geofoam layers for unreinforced and reinforced backfills during the first and last cycles of each loading stage. The highlighted areas in gray and green indicate the stable pressure thresholds for EPS 30 and EPS 20, respectively - thus locating a point inside these regions means it would perform stably under cyclic loading. Previous studies (Ghotbi Siabil et al., 2019) on cubic samples of EPS geofoam with different densities (**Table 1**) had suggested cyclic pressure thresholds of ~140 and ~90 kPa for EPS 30 and EPS 20, respectively. It is clear that all of the points are located inside this safe area, however for the unreinforced case, the stress level of EPS geofoam at the last cycle (red circles) is critically close to the threshold boundary at depths 400 and 600 mm, which signifies the improvement achieved by geocell.

When the lower pressure is applied (in contrast with the second loading stage), amplitudes of P_t are almost equal at various depths of the reinforced and unreinforced installations (the plots are very close) - whether on the first or last load cycle (compare **Fig. 6a** with **Fig. 6b**). During the second loading stage, the pressure transferred to the EPS geofoam layers (especially from surface to a depth of 800 mm) is considerably reduced in the geocell reinforced case, and this reduction is more evident as the loading cycles increase (**Fig. 6b**). Further cycles of load might eventually induce unstable behavior in the pavement foundations due to a steady increase in the intensity of the transferred pressure. The amount of transferred pressure dramatically increases as the applied pressure increases. According to Moghaddas Tafreshi et al. (2014), doubling the applied pressure caused approximately 2.7 times increase in the transferred pressure in depth for both reinforced and unreinforced cases, over the whole range of studied depths. However, the EPS geofoam layer in the unreinforced case experienced more than threefold increase in the transferred pressure.

In all situations, the soil layer plays a significant role in reducing the pressure transferred onto the EPS geofoam. For instance in the first loading cycle of the 275 kPa loading stage, the measured pressure at 400 mm depth of unreinforced and reinforced installations were measured 33.4 and 29.9 kPa, respectively (**Fig. 6a**) – which is equivalent to 88% and 89% reduction from the pressure applied to the surface. On the first load cycle of the second loading stage, the transferred pressures on top of upper EPS layers (depth of 400 mm) were measured as 83.2 and 67.73 kPa for unreinforced and geocell-reinforced cases, respectively (**Fig. 6b**) – which is equivalent to 85% and 88% reduction from the applied pressure; so the difference between reinforced and unreinforced cases is 3% of 550 kPa (16.5 kPa). In the case of highly pressure-sensitive material such as EPS geofoam, this can be a determinant value. With increasing load cycles, the reduction of transferred pressure by geocell becomes considerably evident. Below the uppermost surface of EPS geofoam, the reduction rate of transferred pressure markedly drops with depth (see **Fig. 6a,b**). This can be seen as steeper slopes of the plots at these depths. It can be concluded that the pressure transferred below a depth of 400 mm, whether unreinforced or reinforced, can be assumed equal.

From **Fig. 6**, it could be inferred that the rate of increase in pressure with load cycles varies depending on reinforcement status, intensity of the applied pressure, EPS density in depth (i.e. stable pressure threshold, P_s) and depth of interest. For instance at the depth of 400 mm from pavement surface, the increase in the transferred pressure from cycle 1 to 100 is almost equal for reinforced and unreinforced installations in the first loading stage, while the reinforced pavement performs much better under the second loading stage. Additionally, the rates of increase considerably decreased from top to the bottom of the pavement, specifically below 800 mm depth. The improvement obtained from geocell at depths > 800 mm is negligible for the second loading stage, compared to the first loading stage - which means that such depths are less influenced by the improvement mechanisms geocell provides. In addition, a greater improvement factor by the last load cycle indicates the increased benefit of geocell as strains develop in the system.

6.3 Effect of soil thickness and geocell reinforcement on EPS 30/20

In Test Series 2, the effect of soil reinforcement on EPS 30/20 pavement foundation was evaluated. Thicknesses of the upper and bottom EPS layers were 200 and 600 mm, respectively. The density of the upper and lower EPS layers were 30 and 20 kg/m^3 respectively (see **Table 3**). In the described installations, the overlying soil thicknesses of 400, 500 and 600 mm were tested. In the following subsections, settlements (peak and permanent), the pressure transferred to the EPS geofoam, deflection basin and resilient moduli is elaborated. **Fig. 7** shows the overview of variation in peak and residual settlements of the loading surface and transferred pressure on top of EPS layers, for reinforced and unreinforced cases. It is clear that, when the unreinforced soil thickness is 400 mm, both peak and residual (abbreviated as *Res.* in **Fig. 7b**) settlements increase substantially with a considerable rate, while other cases for thicknesses of 500 and 600 mm show (relatively) stabilizing behavior. As explained in sections 6.1 and 6.2, the reason of unstable behavior for unreinforced pavement foundation is due to the over-stressing on top of EPS 30, as depicted in **Fig. 7c** and **Fig. 6b**.

The effect of geocell reinforcement on surface settlements can be well understood by comparing unreinforced and reinforced cases in **Fig. 7a,b**. Considering h_s = 500 mm at the final load cycle, the peak surface settlement of unreinforced and reinforced pavement foundation is 17.4 and 12.4 mm, respectively. The permanent settlement of unreinforced and reinforced soil for the same situation is 14.9 and 10.6 mm, respectively. This example shows the geocell reinforcement caused up to 29% reduction in the peak and permanent surface settlements for h_s = 500 mm. The reduction in surface settlement due to geocell provision is 35% and 24% for h_s = 400 mm and h_s = 600 mm, respectively. Thus the effectiveness of geocell is dependent on the overlying soil thickness and decreases with increase in the soil thickness. From this figure, it is evident that the geocell reinforced case with h_s = 400 mm shows a larger proportional improvement compared to all of the other unreinforced cases and its performance is comparable to the unreinforced case with h_s = 600 mm. In other words, employing the geocell mattress in the thinnest overlying soil layers (h_s = 400 mm) is equivalent to 50% increase in soil thickness of an unreinforced systems (i.e. h_s = 600 mm).

It is also worth noting that the permanent deformation on the pavement surface (or rut depth) for all cases still remains below the permissible values for low volume roads (50 mm) and major roads (30 mm), as recommended by AASHTO T221-90 (AASHTO 1990), although the reinforced cases are much more promising. The trend of increase suggests that applying additional number of load cycles will not generate deeper ruts on the pavement surface (except in the unreinforced case with h_s = 400 mm).

Variation of the transferred pressure on the top of EPS geofoam (P_t) with number of load cycles is depicted in **Fig. 7c**. For all of the systems examined here, the transferred pressure in the first stage (275 kPa) always remains below 40 kPa (see **Fig. 7**c), which is substantially lower than the threshold cyclic pressure obtained from sample tests on EPS 30 (P_s = 90 kPa as of **Table 1**). With the onset of the second loading stage, the transferred pressure in the unreinforced and reinforced cases of 500 and 600 mm soil remains within stable limits. For the 400 mm soil thickness, the transferred pressure of the unreinforced cases increases substantially at a constants rate (although gradually), while the reinforced case of the same configuration show a relatively constant pressure with number of load cycles.

6.3.1 Improvements in surface settlement and transferred pressure

To assess the improvement achieved from using geocell, the improvement factors (i.e. $IF\delta$ for peak and permanent surface settlement and IFp for the transferred pressure on EPS) of various thicknesses of soil reinforced with geocell at the first and last cycle of each loading stage are displayed in **Fig. 8a** to **Fig. 8c**. When the lower pressure (275 kPa) is applied, the variation of $IF\delta$ and IFp with soil thickness is almost gradual – IF decreases as the soil thickness increases. At this loading stage, $IF\delta$ and IFp are generally below 10% and 5% for all of the soil thicknesses, respectively. The difference in IF between first and last cycle of this loading stage is also negligible. In the first cycle of the second loading stage (550 kPa), the improvement in peak settlement is more pronounced - mostly for the peak settlement of the 400 mm soil thickness, but the improvement in permanent residual deformation is almost similar to smaller pressure stage. However, as more load cycles are applied at this stage, the unreinforced pavement of 400 mm thickness develops large peak and permanent deformations, while the corresponding geocell-reinforced pavement performs much better – resulting in more than 40% improvement.

For the thickness of 500 and 600 and at the first load cycle the geocell reinforcement show small improvement ($IF\delta$ $\leq$10%), but the $IF\delta$ significantly increases at last load .The $IF\delta$ of permanent deformation is close to the $IF\delta$ of peak deformations under the lower applied pressure. In the first loading stage (lower applied pressure), the improvement factors are generally minor – less than 10%. However, the improvement factors grow as the loading repetitions increase, which means that geocell can limit the generation and accumulation of cyclic strains under cyclic loading. When the pavement foundation is subjected to the larger pressure, the geocells have reduced surface settlement by 23% in the first cycle, and up to 41% in the last cycle of this stage. The improvement factors decrease as the overlying soil thickness increases.

Such improvements are delivered in part by reducing the pressures transferred onto the EPS geofoam due to the effect of geocell reinforcement. The transferred pressure improvement, *IFp* is considerable on the second loading stage and increases with increasing load cycles, especially for the thinnest soil layer (400 mm). Similar to the trend observed for surface settlements, the amount of pressure reduction by geocell is also larger under the higher applied pressure. While $IFp_{1,100}$ = 4.99% for soil thickness of 400 mm under 275 kPa cyclic load, $IFp_{2,1}$ = 11.43% when the pavement foundation is subjected to 550 kPa pressure. With increasing number of load cycles, geocell prevents excessive increase in pressure transferred to the EPS geofoam and hence, the absolute values of $IF_{p,1,100}$ are larger than the absolute values of $IF_{p,1,1}$. With increasing soil thickness, the effectiveness of geocell in reducing the pressure transferred to the EPS geofoam diminishes and IF values decrease. At both stages, the increase in transferred pressure with load cycles is significantly lower for the reinforced installation compared to the unreinforced installation.

As discussed in the previous section, the permissible stress limit for EPS 30 is about 90 kPa which is exceeded in the case of the larger applied pressure and thinnest soil cover. The punching shear failure mechanism which develops over a large number of cyclic pressure application is perhaps the main consequence of this exceedance. Reduction in the transferred pressure by means of geocell reinforcement were approximately 5% and 27% for the lower and higher applied pressures, respectively. It can be concluded that geocell reinforcement is capable of reducing both transferred pressure and settlement and its effectiveness increases with increase in the pressure amplitude.

Thus, the data reveals that:

- Incrementally accumulated plastic deformation is far more sensitive to load level than is the magnitude of instantaneous (recoverable) deformation,
- At any particular stress level, the geocell reinforcement has similar effectiveness at limiting both instantaneous and accumulated plastic deformations,
- The geocell reinforcement has a significant effect in reducing such deformations at higher stress (and, hence) strain levels, and,
- For the thicker soil layers, larger shear resistance can be mobilized within the soil layer, resulting in better pressure distribution over EPS. Therefore, the influence of the geocell reinforcement would be greater for

thinner soil layers. A similar trend was also observed by Thakur et al. (2012) for ordinary pavement foundation systems.

Previous studies had demonstrated that geocell pockets provide hoop confinement to the soil, thereby exploiting its passive resistance so as to increase shear strength, distribute stresses and prevent early rupture (Thakur et al., 2012; Moghaddas Tafreshi et al. 2014). Applied above the EPS geofoam, this mechanism helps to avoid localized loading of the EPS geofoam and to avoid large surface settlements, especially with repeated loading application. Under short-term loading the geocell polymers behave almost elastically at high stiffness, trapping energy during loading and then releasing it during unloading, which causes the elastic rebound (resilient deformation) to increase with respect to the total deformation, preventing it from causing failure or rupture in soil. In the absence of geocell reinforcement, the amount of resilient deformation in the EPS geofoam is large, leading to significant shear strain in the overlying soil layer at each cycle and eventually lead to non-stabilizing behavior. By incorporating geocell reinforcement, these large resilient deformations will be moderated, yielding a stiffer response of the whole system.

6.3.2 Deflection basin evaluation

Fig. 9 shows the pavement surface deflection basin on the pavement's surface at the end of the second loading stage. Settlement beyond 600 mm from the center of loading plate was not measured. Thakur et al. (2012) had observed that a slight heave might appear across the settlement profile of unreinforced pavements. This is not apparent in **Fig. 9**, presumably due to the compressibility (without compensating heave) of the EPS geofoam. **Fig. 9** also shows that geocell reinforcement have caused a significant decrease in the final settlement profile. For instance, in the case of 400 mm soil thickness, the peak settlement of about 24 mm in the unreinforced installation decreased to about 16 mm in the case of geocell-reinforced pavement. The insignificant settlement at distance of 600 mm from the center of loading shows that the selected side boundary is sufficient and, therefore, it is expected that the settlement beyond 600 mm from the center would be negligible.

6.3.3 Resilient modulus evaluation

The resilient moduli of soil and EPS under cyclic loading of 0.1 Hz frequency were reported in the ranges of ~200 and ~5 MPa, respectively (Ghotbi Siabil et al., 2019). The exact value for soil and EPS geofoam depend on the compaction of soil and density of EPS geofoam, respectively. For design purposes, it is essential to know the resilient modulus of the composite pavement foundation system. According to **Table 4.**, the resilient moduli depends on the amplitude of loading, thickness of the overlying soil layer and reinforcement status. After a several repetitions of the load cycles, the resilient moduli stabilizes to a constant value, slightly lower than the initial value. Indraratna et al. (2015) also found that that the resilient modulus remained constant at more load repetitions. According to Behiry (2014), the resilient modulus, M_R, from plate load testing is calculated from elastic theory using the following equation:

$$M_R = \frac{\pi(1-\upsilon^2)qa}{2\Delta}$$

Where q is the change in uniformly applied pressure,

υ is the Poisson's ratio of soil,

a is the radius of loading plate,

$\underline{\Delta}$ is the resilient deflection under the loading plate (i.e. the difference between the peak and residual settlement in one particular cycle of loading).

For 275 kPa pressure, the stabilized M_r (on the last loading cycle) is 32.3, 74.9 and 79 MPa for unreinforced soil with thicknesses of 400, 500 and 600 mm, respectively. When the soil is reinforced with geocell, the resilient moduli become 36.2, 86.1 and 90.6 MPa, for the same order of soil thicknesses. When increasing the pressure to 550 kPa, M_r drops to 24% 43% of the values in the previous loading stage. The stabilized (or last cycle) M_r of 400, 500 and 600 mm soil thicknesses are 14.4, 17.3 and 19 for unreinforced status and 22, 23.1 and 23.6 MPa for reinforced soil, respectively. It can be observed that geocell reinforcement has improved the resilient modulus of the 400, 500 and 600 mm soil thickness by 53%, 34% and 24% compared with unreinforced sections. This shows that effectiveness of geocell in improving resilient modulus, reduces with increasing the overlying soil thickness. In agreement, for a totally soil made pavement foundation, Indraratna et al. (2015) and Mengelt et al. (2006) reported up to only 18% increase in the resilient modulus for a geocell-reinforced subballast pavement foundation compared to unreinforced one. The impact of cyclic stress amplitude is evident by comparing the moduli at the two applied pressure levels.

6.4 Effectiveness of geocell reinforcement on reducing density of EPS layers

In order to achieve a cost-effective solution, it would be desirable to reduce the density of EPS layers. However, this might affect the pavement's responses in unfavorable ways. To address the behavior of pavement foundation with lighter EPS, the density of the EPS geofoam layers in the reinforced installations was reduced compared to Test Series 2, and the results were compared with the relevant unreinforced and reinforced cases from Test Series 2 (as benchmark). Due to the incapability of lighter EPS geofoam blocks with thinner soil cover (e.g. 400 mm) in tolerating high pressures (Ghotbi Siabil et al, 2019), only the 600 mm soil thickness was used in the reinforced and unreinforced installations to provide better pressure dispersion on the EPS blocks. The densities of the upper and bottom EPS layers were selected as: γ_{gt} = 30 and γ_{gb} = 20 kg/m^3 (EPS 30/20) in Test Series 2c (unreinforced) and Test Series 2f (reinforced) as benchmark cases, γ_{gt} = 20 and γ_{gb} = 20 kg/m^3 (EPS 20/20) in Test Series 3 (only reinforced) and γ_{gt} = 10 and γ_{gb} = 10 kg/m^3 (EPS 10/10) in Test Series 5 (only reinforced), as provided in **Table 3**.

Variation in the peak and residual settlements of loading surface with respect to the number of load cycles are shown in Error! Reference source not found.**a** and **Fig. 10b**, respectively. Even though the reinforced soil on EPS 10/10 seems to have performed well in the first loading stage, more than 70 mm of settlement and consequent failure occurs in the pavement surface after only 180 cycles of the second loading stage (only up to 20 mm and 16 mm peak and residual settlements under the few first cycles are shown respectively in Fig. 10a and Fig. 10b). From Error! Reference source not found.**c**, such failure is coincident with a constant increase in the pressure transferred to the top of EPS geofoam layer (EPS 10), initiating from the beginning of the second loading stage. This observation is similar to what happens when a geocell layer is placed over a void. Sireesh et al., 2009 explain that due to very low end bearing resistance from presence of the void, geocell mattress did not provide a noteworthy improvement in the performance and the geocell mattress punched into the void. They also explained that the negligible performance improvement caused by geocell inclusion was the results of skin friction mobilized on the external surface of geocell mattress, similar to piles. A similar phenomenon is observed in the case of the pavement foundation on EPS 10.

It can be observed that, although unreinforced EPS 30/20 performs very similarly to reinforced EPS 20/20 in the first loading stage, its settlement eventually overtakes that of the reinforced 20/20 case in the second loading stage (Error! Reference source not found.**a,b**). Despite lighter/softer EPS geofoam involved in the EPS 20/20 reinforced case compared to the unreinforced EPS 30/20, less cyclic deformation is accumulated as load cycles increase, compensating the effect of the softer underlying bed. Thus, the reinforced EPS 20/20 could be incorporated instead of unreinforced EPS 30/20, depending on project costs and requirements.

6.4.1 Improvements in surface settlement and transferred pressure

Table 5 displays the improvement factors pertaining to settlements and transferred pressures for the above described schemes, compared to the unreinforced pavement foundation of EPS 30/20 (as benchmark). On the first loading stage, the improvement of reinforced EPS 20/20 and EPS 30/20 pavement foundations are less significant compared to unreinforced EPS 30/20 (absolute value of $IF_{\delta,1,100}$ is less than 5 %); while the reinforced EPS 10/10 is not only improved compared to unreinforced EPS 30/20, but also a noticeable increase (57.8%) was observed in the surface settlement. On the first cycle of the second loading stage, $IF_{\delta,2,1}$ = 10.97 % and 5.48 % for reinforced EPS 30/20 and EPS 20/20, respectively. Similar to the previous loading stage, the surface settlement grows even greater for the reinforced EPS 10/10 - up to $IF_{\delta,2,1}$= -127%. As the load cycles increase, the reinforced pavement foundation on EPS 20/20 shows an acceptable performance compared to unreinforced pavement foundation on EPS 30/20 and thus, it can serve as an appropriate alternative, considering project costs. Regarding the change in pressure ratios, the transferred pressure ratio for reinforced EPS 20/20 is slightly larger compared to the benchmark case (IFp = 6.3-13%), but still within the safe stress limit (**Table 1.**).

Hence, it is evident that provision of geocell reinforcement in the soil above EPS geofoam can provide sufficient bearing capacity increase to compensate for softer EPS geofoam underlain, but only within certain limits. Once the EPS geofoam becomes too soft (i.e. EPS 10), then the modest soil reinforcement provided by the geocells is a grossly inadequate replacement for the loss of capacity that destructive failure of a low capacity EPS geofoam undergoes.

6.5 Effectiveness of geocell reinforcement on reducing soil thickness on EPS 20/20

According to **Section 6.4**, pavement foundations with 600 mm geocell-reinforced soil supported on EPS geofoam lighter than 20 kg/m^3 (i.e. EPS 10/10) experience accelerated increase in rut depths under repetitive loading - resulting in pavement failure. Yet, reduction of the overlying soil thickness might be demanding in some circumstances. Hence in Test Series 3 and 4, thickness of the reinforced soil layer was reduced, and the results were compared with the results of 600 mm thick (maximum tested thickness) unreinforced soil as the benchmark, all on EPS 20/20. The overall thickness of EPS bed was equal to 800 mm and the thickness of soil layer varied from 600 to 400 mm for geocell-reinforced installation. **Fig. 11a,b** show peak and residual settlements of the loading surface for the described pavement foundations.

At both loading stages, the reinforced soil with thickness of 500 and 600 mm evidently exhibited a better performance compared to unreinforced soil with thickness of 600 mm. At the lower applied pressure, settlements in the unreinforced case with thickness of 600 mm are slightly smaller compared to the reinforced case with a soil thickness of 400 mm (similar to initial cycles of the higher applied pressure), but the rate of increase becomes larger in the second loading stage and the settlement soon exceeds those of the reinforced case. As it is shown in **Fig. 11c**, the transferred pressure in the installation with unreinforced soil 600 mm thick increases beyond the stable pressure threshold of EPS 20, which is in agreement with the variation in settlement. The transferred pressure in the reinforced cases remain within a safe limit for all of the soil thicknesses. Therefore, the value of reinforcement of a soil layer above low density EPS geofoam beds is clearly demonstrated.

6.5.1 Improvements in surface settlement and transferred pressure by geocell

A detailed summary of improvement factors is reported in **Table 6**. The results of reinforced pavement foundations with different thicknesses are compared with the unreinforced foundation of 600 mm soil thickness as benchmark. On the first loading stage, the settlements of reinforced 600 mm soil cases are obviously lower. The reinforced pavement with h_s = 600 and 500 mm show approximately 30% and 16% lower peak settlements compared to benchmark case. However, the peak settlements of 400 mm reinforced case are 24% larger than those of the benchmark case. When the applied pressure is increased to 550 kPa, even the performance of the 400 mm reinforced pavement foundation gets slightly better on the first cycle and, with increasing load cycles, the reinforced EPS 20/20 has even greater performance ($IF_{\delta,2,400}$ = 19.59%). As explained in previous sections, these behaviors can be easily interpreted by comparing the transferred pressure values (**Fig.**

11c). The improvement delivered from reinforcing a 600 mm thick overlying soil is greatest. For instance, a 43.6% decrease in pressure is observed at the final cycle of the second loading stage. With decreasing soil thickness, the improvement reduces, so that at the first loading stage of 400 mm soil thickness, no improvement is observed. Although by the last load cycles of the second loading stage, the geocell reduces the surface settlement by 19.51%.

Thus with the thinnest soil cover, reinforcement has a small benefit at low applied stresses and, initially, at higher stresses. At all other stress levels, and at the higher stress after 400 cycles of loading, a significant benefit of the reinforcement is seen for all soil thicknesses. Thus, it seems that installation of the reinforcement locally degrades initial response (presumably due to bedding and/or geocell tensioning effects). Yet this small effect is not noticeable in thicker soil layers where (apparently) it is a smaller part of the overall reinforcement benefit, nor at higher stresses/strains where geocell tensioning (and, hence, reinforcement) benefit becomes more significant.

7 Simplified numerical simulation

Alongside experiments, a series of numerical analyses was performed to improve the understanding of the response of EPS geofoam pavements reinforced with geocell. According to the results of laboratory tests, the major portion of surface settlements occurs during the first cycle of loading, irrespective of the loading stage. Consequently simulating the first load cycle could provide valuable insight regarding the mechanisms involved. Thus to prevent lengthy and complicated computational effort, the numerical simulation was limited to the first cycle of each loading stage (275 kPa and 550 kPa cyclic pressures). Using these assumptions, settlement that resulted from an applied single cycle of 550 kPa load in the numerical analysis, can be compared to the experimental settlement under the first cycle in the second loading stage – i.e. when the settlements during cycle 2 to 100 from the first loading stage of experiments were excluded. It has to be noted that such numerical analysis does not aim to predict the behavior during the whole loading cycles, but rather to give an overall overview of the mechanisms, stress and settlement contours and interaction between soil, geocell and EPS geofoam bed using the above assumptions.

7.1 Description

The numerical simulation was performed using a 3D finite element model created in ABAQUS software (Simulia, D.S., 2013). The overall method of modeling used here was previously employed and verified by Leshchinsky and Ling (2013b) and Satyal et al. (2018). To capture the behavior of soil and EPS geofoam, a Drucker-Prager constitutive law was employed with the parameters presented in **Table 7.** In agreement with the experience of the authors during numerical simulations, Jian and Xie (2011) reported that although the Mohr-Coulomb (M-C) is a normally accepted criterion within the geotechnical engineering field, but it has two major limitations that prevent its widespread usage. First, and in contrast with test results on the strength of material, the yield strength of material is underestimated when M-C is employed. This is due to the neglecting the constraining effect of the intermediate principal stress. Second, the projection of the M-C yield surface on the deviatoric stress plane comprises six sharp corners of an irregular hexagon with non-identical partial derivatives, which induces certain problems to the convergence in flow theory. The results of previous triaxial tests with three confining pressures on soil samples were used to calibrate the parameters required for soil modeling. To obtain values for EPS geofoam, uniaxial compression tests and triaxial compression tests were performed on cubic samples of each EPS density. The Poisson's ratio of EPS geofoam was selected based on the suggestions of previous research (e.g. Ossa and Romo, 2009; Trandafir et al., 2010). In the Drucker-Prager model used in ABAQUS, an additional parameter, termed the flow stress ratio, is used to modify the yield criterion for c- φ material. The flow stress ratio is defined as the flow stress for the case of triaxial extension divided by that for triaxial compression. By this means the influence of the intermediate principal stress on the yield surface can be incorporated. The samples were thus modeled in ABAQUS and appropriate values were calibrated to obtain a close match with the experimental data. However, larger EPS blocks would show larger elastic moduli (or resilient moduli) compared to smaller samples (also reported by Negussey, 2007). Therefore, the final parameter values were doubled to produce acceptable results.

A penalty method with tangential coefficient of 0.4 was used to model the frictional behavior between soil and EPS geofoam. As no penetration is expected to happen between the soil and EPS geofoam, their normal interaction was considered as rough. For the soil and geofoam, 8-node 3D 'brick' elements (C3D8R) were used while, the geocell was modeled in its realistic geometry using 4-node quadrilateral, reduced integration elements with 'hourglass control' (M3D4R) using a linear elastic model. It is expected that the geocell joints have a strength no lower than the parent geocell fabric. Also, being a small proportion of the fabric, any increase in strength will not have a noticeable effect on the whole. Thus, the joints were not specifically modeled. A similar approach was chosen by other researchers (e.g. Leshchinsky and Ling, 2013b; Oliaei and Kouzegaran, 2017; Satyal et al., 2018). The geocell elements were connected to the soil region using the embedment formulation available in ABAQUS. This method introduces an interface friction corresponding to the internal friction angle of the infill material, a behavior that has been determined by former research studies (Biabani and Indraratna, 2015; Indraratna et al., 2011; Yang et al., 2010). The loading plate was modeled by shell elements with large stiffness and its interaction with soil layer was established by penalty for frictional and rough for normal behaviors. Using a static procedure, the pressure of each loading stage was applied to the loading plate in 5 seconds as a haversine with pulse length of 10 seconds (5 seconds corresponds to peak time of 0.1 Hz frequency used in laboratory tests). To save computer time, only one quarter of the test model was created with nodes on the planes of symmetry fixed in the direction perpendicular to the plane, but free to move in other directions. For the external side boundaries, only vertical movements were free. The bottom boundary was fixed in all of the directions. A graphical illustration of the total model assembly including soil and EPS layers, geocell layer and loading plate and their corresponding Finite Element mesh along with an illustration of the one-time static loading used in the numerical analyses are shown in **Fig. 12**.

7.2 Validation

Fig. 13 compares the results of the numerical simulation with the experiments (Test Series 2) for the three thicknesses of unreinforced and geocell-reinforced pavement foundations (h_s = 400, 500 and 600 mm). Based on the explanations on the beginning of **Section 7** (i.e. the major portion of surface settlements at the first loading stage occurs during the first cycle of loading) and in order to make the numerical and experimental results comparable, the effect of cyclic loading occurred at the first loading stage from cycle 2 to 100 were excluded from the original experimental results. The general trend of numerical simulation is similar to the experimental results, especially for the lower applied pressure. For the 550 kPa applied pressure, a slight variation can be observed in the numerical results. Application of 100 cycles of lower pressure might have compacted the granular medium and increased (although insignificantly) the soil's stiffness. By this explanation the physical soil layer can dissipate pressure to a wider area, resulting in greater load spreading and smaller settlements than expected at the higher stress level. The mismatch is more evident for lower thicknesses of soil, as the numerical h_s=500 and 600 mm models already encompass this phenomenon (better load spreading and reduced settlement) due to their larger thickness. Therefore, the numerical model can provide fairly accurate replicate results of the physical test results.

7.3 Model results

7.3.1 Settlements and strains in EPS geofoam

To determine the reaction of soil and EPS layers to the applied pressure individually, the settlement profile of each layer at the end of 550 kPa pressure application is plotted in **Fig. 14**. According to these plots, for the locations around the loading plate (approximately up to 200 mm from the center to each side), the settlements of the pavement surface and the upper EPS layer are markedly different between reinforced and unreinforced installations. In this region, the settlement of the soil layer has increased as a consequence of increase in the settlement of the underlain upper EPS layer. Beyond this central zone, the settlement of the soil surface and upper EPS layer are approximately equal for both of the reinforcement states. The settlement of the bottom EPS layer at 600mm is almost the same for both unreinforced and reinforced cases, and doesn't vary much along the side of the pavement – indicating the effectiveness of the overlying layers. The increase in the soil settlement near the loading axis is due to the significant deformation of EPS geofoam and is located between the inflexion points of the settlement plot for the upper EPS layer (400mm depth). Geocell reinforcement has reduced the settlement of EPS geofoam due to its pressure spreading mechanisms and this has led to a consequent reduction in the settlement of the soil surface. In other words, the concentrated form of settlement (encompassing possible failure in the

EPS geofoam) in the unreinforced case has been transformed to much smaller uniform settlements over a wider area of EPS geofoam layer. This effect certainly assists in an increase in the service life of the pavement.

Based on the observations during tests (**Fig. 1**) and the numerical analysis (**Fig. 14**), two major failure mechanism can be distinguished in geocell-reinforced and unreinforced pavement foundations supported on EPS geofoam blocks:

(1) *Punching failure mechanism:* The punching failure mainly occurs in the unreinforced situation; when the thickness of the overlying soil layer is insufficient (perhaps when h_s<400 mm). When the overlying soil layer is reinforced with geocell, it mainly happens when the EPS density is very low (γ_{gt} and γ_{gb} < 20 kg/m^3).

(2) *Global/local shear failure mechanism:* When the overlying soil is thick and EPS geofoam is competent, it is expected that the deformation of EPS geofoam surface below the soil cover is negligible and a full shear failure can be formed.

The mentioned failure mechanisms and suggested bounds for occurring them is almost qualitative and can be used as rule of thumb for design purposes. An exact categorization must include the effect of more factors including soil type, soil compaction and geocell characteristics.

7.3.2 Strains in geocell

The longitudinal strains in the geocell of the pavement foundations with h_s=600 mm and with soil constructed on EPS 20/20 or EPS 30/20 are shown **Fig. 15a** and **Fig. 15b**, respectively. According to these plots, the geocell layer has undergone larger vertical settlement in the case of the EPS 20/20 pavement compared to that in the EPS 30/20. Due to the generation of tensile stress at the bottom surface of geocell layers acting in bending, the longitudinal strain is significantly larger at the bottom of both geocell layers than elsewhere. The peak value of tensile strain varies depending on the density of the supporting EPS layers and the amount of consequent settlement encountered by the geocell layer. For EPS 30/20 case, the peak strain is around 0.41%, while for EPS 20/20, the strain value can increase up to 0.63%. The deformed shape of geocell also indicates the large settlement occurring from lower density of the EPS layers.

8 Conclusion

To prevent EPS geofoam failure or long-term settlement of the embankment requires sufficient spreading of loads imposed at the ground surface so that the stresses on the EPS are not too large. This could be achieved by thick soil layers, but that’s not desirable as it increases the embankment mass – while the purpose of the EPS was to reduce it. So more effective load spreading using a geocell reinforcement in a thin covering soil layer could be a competent method for improving the performance of the pavement foundation. Using large-scale cyclic plate testing and a simplified Finite Element analysis in this study, the benefits of incorporating geocell in the soil layer overlying EPS geofoam backfills was assessed. The effect of geocell reinforcement on surface settlements, amplitude of the pressure transferred to the EPS geofoam and resilient modulus of the system was studied for different thicknesses of soil and different EPS densities. The following outcomes have been obtained:

(1) Use of a geocell over EPS geofoam is best when the stress likely to be experienced by the EPS geofoam would be excessive. When employing geocell reinforcement in the thinner soil layers, an improvement can be obtained equivalent to a 50% increase in soil thickness.

(2) As the surface applied pressure increases, the increase in the pressure within EPS geofoam layers of an unreinforced system may be larger than the increase experienced by ordinary soil. For example, when doubling the applied pressure (from 275 to 550 kPa), the transferred pressure in the EPS layers triples. Using geocell reinforcement in the soil above EPS geofoam would prevent the excessive increase in the pressure amplitude within EPS layers.

(3) The deflection basins (physical and computed) give some indication that the mode of failure in the EPS geofoam would involve punching into the geofoam. The provision of reinforcement in the covering soil helps to reduce settlement concentration, spreading the settlements over a wider area.

(4) Incrementally accumulated plastic deformation is far more sensitive to load level in the composite systems evaluated than is the magnitude of instantaneous (recoverable) deformation.

(5) Using geocell reinforcement, the resilient modulus of the reinforced EPS backfilled system is raised significantly from the unreinforced case, resulting in lower transient deflections. As much as 53% increase in the resilient modulus of pavements on EPS geofoam is obtained, which is significant compared to the 18% increase for geocell-reinforced pavements without EPS geofoam.

(6) Geocell-reinforced pavement foundations with EPS 20/20 can be selected as suitable alternatives to EPS 30/20, but EPS 10/10 failed very rapidly except when in a low pressure situation, even when under a geocell-reinforced 600 mm thick soil layer.

(7) Using geocell reinforcement can compensate for the effect of reduced soil cover, particularly on the softer EPS geofoam.

(8) The degree of effectiveness of using geocell on the soil above EPS geofoam is dependent on the soil thickness. With decreasing soil thickness, effectiveness of geocell reinforcement considerably increases.

(9) Using a simple numerical analysis, it can be concluded that the major reason for collapse of the pavement with EPS geofoam is the high deformability of EPS geofoam under the applied pressure which in some cases results in lack of support and punching failure. Geocell can spread the pressure over a wider zone and hence reduce premature failures.

The current research is assisting the understanding of the effect of geocell reinforcement in improving the performance of road pavement foundations encompassing EPS geofoam blocks. As only one type of EPS geofoam and one type of geocell were used, the results might be subject to change if using materials with properties other than those introduced here. The numerical simulation is also limited to the first cycle of loading stages using simplifying assumptions. Nevertheless, the observed trends are not expected to dramatically change for similar configurations to those used here. Considering these limitations, the results obtained here must be exploited with caution for practical applications. Future studies could extend this work to improve current guidelines by considering other types of soil, EPS material and different stiffness and geometry of geocell reinforcement. Further numerical studies can also be performed considering cyclic loading application.

Acknowledgment

The authors appreciate cooperation of DuPont de Nemours, Luxembourg, and their UK agents, TDP Limited for supplying geocell reinforcements used in the testing program.

Nomenclature

a	Radius of loading plate
D	Diameter of the loading plate
h_s	Thickness of soil layer
h_{gt}	Thickness of upper EPS geofoam layer
h_{gb}	Thickness of bottom EPS geofoam layer
γ_{gb}	Density of bottom EPS geofoam layer
γ_{gt}	Density of upper EPS geofoam layer
γ_s	Density of soil
$\delta_{r.m.n}$:	Surface settlement (mm).
$p_{r.m.n}$:	Vertical stress at point of interest (kPa).
P_s:	Stable pressure threshold of EPS geofoam.
P_t:	Pressure transferred on EPS geofoam.
X:	Reinforcement status (r for reinforced and u for unreinforced).
n:	Number of load cycles, the cycle number is reset to 1 for the first cycle of the second, more highly loaded, stage (1, 101 and 400 indicate the first cycle of both loading stages, last cycle of first loading stage and the last cycle of second loading stage, respectively).
M_R	Resilient modulus
q	Change in uniformly applied pressure
j, k:	Value of n at first and last cycle of loading, respectively
m:	1 and 2 for the first and second loading stages (applied pressures of 275 and 550 kPa to loading plate), respectively
IFp	Improvement factor for comparison of reinforced and unreinforced transferred pressures
IFδ	Improvement factor for comparison of reinforced and unreinforced settlements
υ	Poisson’s ratio
Δ	Resilient deflection under the loading plate

References

American Association of State Highway and Transportation Officials (AASHTO), 1990. Repetitive static plate load tests of soils and flexible pavement components for use in evaluation and design of airport and highway pavements. AASHTO T 221-90. Washington, DC.

AbdelSalam, S. S., Azzam, S. A., 2016. Reduction of lateral pressures on retaining walls using geofoam inclusion. Geosynth. Int. 23(6), 395-407. https://doi.org/10.1680/jgein.16.00005.

AbdelSalam, S. S., Jama, R. A., Salah, M. A., 2019. EPS inclusion to reduce vertical stresses on shallow tunnels. Geosynth. Int. 26 (2), 121-135. https://doi.org/10.1680/jgein.18.00042.

Abdollahi, M., Moghaddas Tafreshi, S. N., Leshchinsky, B., 2019. Experimental and Numerical Assessment of Geogrid-EPS Geofoam Systems for Protecting Buried Utilities. Geosynth. Int. 26(4), 333-353. https://doi.org/10.1680/jgein.19.00013.

Abu-Farsakh, M., Hanandeh, S., Mohammad, L., Chen, Q., 2016. Performance of geosynthetic reinforced/stabilized paved roads built over soft soil under cyclic plate loads. Geotext. Geomembranes 44(6), 845-853. https://doi.org/10.1016/j.geotexmem.2016.06.009.

Akay, O., Özer, A. T., Fox, G. A., Bartlett, S. F., Arellano, D., 2013. Behavior of sandy slopes remediated by EPS-block geofoam under seepage flow. Geotext. Geomembranes, 37, 81-98. https://doi.org/10.1016/j.geotexmem.2013.02.005.

Akay, O., Özer, A. T., Fox, G. A., 2014. Assessment of EPS block geofoam with internal drainage for sandy slopes subjected to seepage flow. Geosynth. Int. 21(6), 364-376. https://doi.org/10.1680/gein.14.00024.

Akay, O., 2015. Slope stabilisation using EPS block geofoam with internal drainage system. Geosynth. Int. 23(1), 9-22. https://doi.org/10.1680/jgein.15.00028.

Anil, Ö., Erdem, R. T., Kantar, E., 2015. Improving the impact behavior of pipes using geofoam layer for protection. Int. J. Pres. Ves. Pip. 132, 52-64. https://doi.org/10.1016/j.ijpvp.2015.05.007

Arulrajah, A., Piratheepan, J., Disfani, M. M., Bo, M. W., 2012. Resilient moduli response of recycled construction and demolition materials in pavement subbase applications. J. Mater. Civil Eng. 25(12), 1920-1928.

Arulrajah, A., Piratheepan, J., Disfani, M., 2014. Reclaimed asphalt pavement and recycled concrete aggregate blends in pavement subbases: laboratory and field evaluation. J. Mater. Civil Eng. 26(2), 349-357.

Arulrajah, A., Piratheepan, J., Disfani, M., Bo, M., 2013. Resilient moduli response of recycled construction and demolition materials in pavement subbase applications. J. Mater. Civil Eng. 25(12), 1920-1928.

Arulrajah, A., Yaghoubi, E., Wong, Y.C., Horpibulsuk, S. 2017. Recycled plastic granules and demolition wastes as construction materials: Resilient moduli and strength characteristics. Constr. Build. Mater. 147, 639-647. https://doi.org/10.1016/j.conbuildmat.2017.04.178.

American Society for Testing and Materials, 2007. Standard Test Method for Density and Unit Weight of Soil in Place by the Sand-Cone Method. ASTM Int'l D1556-07.

American Society for Testing and Materials, 2009. Standard Test Method for Repetitive Static Plate Load Tests of Soils and Flexible Pavement Components, for Use in Evaluation and Design of Airport and Highway Pavements. ASTM Int'l D1195-09.

American Society for Testing and Materials, 2012. Standard Test Methods for Laboratory Compaction Characteristics of Soil Using Modified Effort. ASTM Int'l D1557-12.

American Society for Testing and Materials, 2000. Standard Test Method for Compressive Properties of Rigid Cellular Plastics. ASTM Int'l D1621-00.

American Society for Testing and Materials, 2008. Standard Test Method for Apparent Density of Rigid Cellular Plastics. ASTM Int'l D1622-08.

American Society for Testing and Materials, 2011. Standard Practice for Classification of Soils for Engineering Purposes (Unified Soil Classification System). ASTM Int'l D2487-11.

American Society for Testing and Materials, 2015. Standard Test Method for Unconsolidated-Undrained Triaxial Compression Test on Cohesive Soils. ASTM Int'l D2850-15.

American Society for Testing and Materials, 2009. Standard Specification for Graded Aggregate Material for Bases or Subbases for Highways or Airports. ASTM Int'l D2940-09.

American Society for Testing and Materials, 2005. Standard Guide for Use of Expanded Polystyrene (EPS) Geofoam in Geotechnical Projects. ASTM Int'l D7180-05.

Athanasopoulos, G. A., Pelekis, P. C., Xenaki, V. C., 1999. Dynamic properties of EPS geofoam: an experimental investigation. Geosynth. Int. 6(3), 171-194. https://doi.org/10.1680/gein.6.0149.

Barrett, J. C., Valsangkar, A. J., 2009. Effectiveness of connectors in geofoam block construction. Geotext. Geomembranes 27(3), 211-216. https://doi.org/10.1016/j.geotexmem.2008.11.010.

Bartlett, S. F., Lingwall, B. N., Vaslestad, J., 2015. Methods of protecting buried pipelines and culverts in transportation infrastructure using EPS geofoam. Geotext. Geomembranes 43(5), 450-461. https://doi.org/10.1016/j.geotexmem.2015.04.019.

Bathurst, R. J., Zarnani, S., Gaskin, A., 2007. Shaking table testing of geofoam seismic buffers. Soil Dyn. Earthq. Eng. 27(4), 324-332. https://doi.org/10.1680/gein.2007.14.3.165.

Behiry, A. E. M., 2014. Characterization of the layered pavement by modelling and calibration of resilient modulus. American Journal of Civil Engineering 2(3), 74-86.

Beju, Y. Z., Mandal, J. N., 2017. Combined Use of Jute Geotextile-EPS Geofoam to Protect Flexible Buried Pipes: Experimental and Numerical Studies. International Journal of Geosynthetics and Ground Engineering 3(4), 32. https://doi.org/10.1007/s40891-017-0107-5.

Biabani, M. M., Indraratna, B., 2015. An evaluation of the interface behaviour of rail subballast stabilised with geogrids and geomembranes. Geotext. Geomembranes 43(3), 240-249. https://doi.org/10.1016/j.geotexmem.2015.04.002.

Biabani, M. M., Indraratna, B., Ngo, N. T., 2016a. Modelling of geocell-reinforced subballast subjected to cyclic loading. Geotext. Geomembranes 44(4), 489-503. https://doi.org/10.1016/j.geotexmem.2016.02.001.

Biabani, M. M., Ngo, N. T., Indraratna, B., 2016b. Performance evaluation of railway subballast stabilised with geocell based on pull-out testing. Geotext. Geomembranes 44(4), 579-591. https://doi.org/10.1016/j.geotexmem.2016.03.006.

Biswas, A., Murali Krishna, A., Dash, S. K., 2013. Influence of subgrade strength on the performance of geocell-reinforced foundation systems. Geosynth. Int. 20(6), 376-388. https://doi.org/10.1680/gein.13.00025.

Brito, L. A. T., Dawson, A. R., Kolisoja, P. J., 2009. Analytical evaluation of unbound granular layers in regard to permanent deformation. Proceedings of the 8th International on the Bearing Capacity of Roads, Railways, and Airfields (BCR2A'09), Champaign IL, USA, 187-196.

Chen, R. H., Huang, Y. W., Huang, F. C., 2013. Confinement effect of geocells on sand samples under triaxial compression. Geotext. Geomembranes 37, 35-44. https://doi.org/10.1016/j.geotexmem.2013.01.004.

Choudhary, A. K., Pandit, B., Babu, G. S., 2019. Uplift capacity of horizontal anchor plate in geocell reinforced sand. Geotext. Geomembranes 47(2), 203-216. https://doi.org/10.1016/j.geotexmem.2018.12.009.

Collins, I. F., Boulbibane, M., 2000. Geomechanical analysis of unbound pavements based on shakedown theory. J. Geotech. Geoenvironmental Eng. 126(1), 50-59.

Dash, S. K., Choudhary, A. K., 2018. Geocell reinforcement for performance improvement of vertical plate anchors in sand. Geotext. Geomembranes 46(2), 214-225. https://doi.org/10.1016/j.geotexmem.2017.11.008.

De, A., Morgante, A. N., Zimmie, T. F., 2016. Numerical and physical modeling of geofoam barriers as protection against effects of surface blast on underground tunnels. Geotext. Geomembranes 44(1), 1-12. https://doi.org/10.1016/j.geotexmem.2015.06.008.

DeMerchant, M. R., Valsangkar, A. J., Schriver, A. B., 2002. Plate load tests on geogrid-reinforced expanded shale lightweight aggregate. Geotext. Geomembranes 20(3), 173-190. https://doi.org/10.1016/S0266-1144(02)00006-7.

Donrak, J., Rachan, R., Horpibulsuk, S., Arulrajah, A., Du, Y.J., 2016. Improvement of marginal lateritic soil using Melamine Debris replacement for sustainable engineering fill materials. J. Clean Prod. 134, 515-522. https://doi.org/10.1016/j.jclepro.2015.12.038.

Duškov, M., 1997a. Materials research on EPS20 and EPS15 under representative conditions in pavement structures. Geotext. Geomembranes 15(1-3), 147-181. https://doi.org/10.1016/S0266-1144(97)00011-3.

Duškov, M., 1997b. Measurements on a Flexible Pavement Structure with an EPS Geofoam Sub-Base. Geotext. Geomembranes 15(1-3), 5-27. https://doi.org/10.1016/S0266-1144 (97)00011-3.

El-kady, M. S., Alzara, M. A., Farouk, M. A., 2018. Reduction of lateral earth pressure using Geo-foam blocks. Innov. Infrastruct. Solut. 3(1), 40. https://doi.org/10.1007/s41062-018-0145-4.

Ertugrul, O. L., Trandafir, A. C. 2011. Reduction of lateral earth forces acting on rigid nonyielding retaining walls by EPS geofoam inclusions. J. Mater. Civil Eng. 23(12), 1711-1718.

Farnsworth, C. B., Bartlett, S. F., Negussey, D., Stuedlein, A. W., 2008. Rapid construction and settlement behavior of embankment systems on soft foundation soils. J. Geotech. Geoenvironmental Eng. 134(3), 289-301. https://doi.org/10.1061/(ASCE)1090-0241(2008)134:3(289).

Fazeli Dehkordi, P., Ghazavi, M., Ganjian, N., Karim, U. F. A., 2019. Effect of geocell-reinforced sand base on bearing capacity of twin circular footings. Geosynth. Int. 1-13. https://doi.org/10.1680/jgein.19.00047.

Gandahl, R., 1988. Polystyrene foam as a frost protection measure on national roads in Sweden. Transportation Research Record (1146), 1-9.

Gao, H., Bu, C., Wang, Z., Shen, Y., Chen, G., 2017a. Dynamic characteristics of expanded polystyrene composite soil under traffic loadings considering initial consolidation state. Soil Dyn. Earthq. Eng. 102, 86-98. https://doi.org/10.1016/j.soildyn.2017.08.012

Gao, H., Hu, Y., Wang, Z., Wang, C., Chen, G., 2017b. Shaking table tests on the seismic performance of a flexible wall retaining EPS composite soil. B. Earthq. Eng. 15(12), 5481-5510. https://doi.org/10.1007/s10518-017-0189-4.

Georgees, R. N., Hassan, R. A., Evans, R. P., Jegatheesan, P., 2018. An evaluation of performance-related properties for granular pavement materials using a polyacrylamide additive. Int. J. Pavement Eng. 19(2), 153-163. https://doi.org/10.1080/10298436.2016.1172710.

Ghotbi Siabil, S. M. A., Moghaddas Tafreshi, S. N., Dawson, A. R., Parvizi Omran, M., 2019. Behavior of expanded polystyrene (EPS) blocks under cyclic pavement foundation loading. Geosynth. Int. 26(1), 1-25. https://doi.org/10.1680/jgein.18.00033.

Gnanendran, C. T., Piratheepan, J., Ramanujam, J., Arulrajah, A., 2011. Accelerated laboratory pavement model test on cemented base and clay subgrade. Geotech. Test J. 34(4), 297-309. https://doi.org/10.1520/GTJ103311.

Gonzalez-Torre, I., Calzada-Perez, M. A., Vega-Zamanillo, A., Castro-Fresno, D., 2015. Evaluation of reflective cracking in pavements using a new procedure that combine loads with different frequencies. Constr. Build. Mater. 75, 368-374. https://doi.org/10.1016/j.conbuildmat.2014.11.030.

Hazarika, H., Okuzono, S., 2004. Modeling the behavior of a hybrid interactive system involving soil, structure and EPS geofoam. Soils Found. 44(5), 149-162.

Hazarika, H., 2006. Stress–strain modeling of EPS geofoam for large-strain applications. Geotext. Geomembranes, 24(2), 79-90. https://doi.org/10.1016/j.geotexmem.2005.11.003.

Hegde, A., 2017. Geocell reinforced foundation beds-past findings, present trends and future prospects: A state-of-the-art review. Constr. Build. Mater. 154, 658-674. https://doi.org/10.1016/j.conbuildmat.2017.07.230.

Hegde, A. M., Sitharam, T. G., 2015a. 3-Dimensional numerical modelling of geocell reinforced sand beds. Geotext. Geomembranes 43(2), 171-181. https://doi.org/10.1016/j.geotexmem.2014.11.009.

Hegde, A. M., Sitharam, T. G., 2015b. Three-dimensional numerical analysis of geocell-reinforced soft clay beds by considering the actual geometry of geocell pockets. Can. Geotech. J. 52(9), 1396-1407. https://doi.org/10.1139/cgj-2014-0387.

Hegde, A. M., Sitharam, T. G., 2015c. Experimental and numerical studies on protection of buried pipelines and underground utilities using geocells. Geotext. Geomembranes 43(5), 372-381. https://doi.org/10.1016/j.geotexmem.2015.04.010.

Hegde, A., Sitharam, T. G., 2017. Experiment and 3D-numerical studies on soft clay bed reinforced with different types of cellular confinement systems. Transp. Geotech. 10, 73-84. https://doi.org/10.1016/j.trgeo.2017.01.001.

Horvath, J. S., 1994. Expanded polystyrene (EPS) geofoam: an introduction to material behavior. Geotext. Geomembranes 13(4), 263-280. https://doi.org/10.1016/0266-1144(94)90048-5.

Horvath, J. S., 1997. The compressible inclusion function of EPS geofoam. Geotext. Geomembranes 15(1-3), 77-120.

Horvath, J. S., 2010. Emerging trends in failures involving EPS-block geofoam fills. J. Perform. Constr. Fac. 24(4), 365-372. https://doi.org/10.1061/(ASCE)CF.1943-5509.0000114.

Huang, Y.H., 1993. Pavement analysis and design. Englewood Cliffs, NJ: Prentice Hall, http://worldcat.org/isbn/0136552757.

Indraratna, B., Hussaini, S. K. K., Vinod, J. S., 2011. On the shear behavior of ballast-geosynthetic interfaces. Geotech. Test J. 35(2), 305-312. https://doi.org/10.1520/GTJ103317.

Indraratna, B., Biabani, M. M., Nimbalkar, S., 2015. Behavior of geocell-reinforced subballast subjected to cyclic loading in plane-strain condition. J. Geotech. Geoenvironmental Eng. 141(1), https://doi.org/10.1061/(ASCE)GT.1943-5606.0001199.

Jegatheesan, P., Gnanendran, C. T., 2015. Permanent Deformation Study of Pavement Layers Using Laboratory Pavement Model Testing. Int. J. Geomech. 16(3), 04015072.

Jiang, H., Xie, Y., 2011. A note on the Mohr–Coulomb and Drucker–Prager strength criteria. Mech. Res. Commun. 38(4), 309-314. https://doi.org/10.1016/j.mechrescom.2011.04.001.

Keller, G. R., 2016. Application of geosynthetics on low-volume roads. Transp. Geotech. 8, 119-131. https://doi.org/10.1016/j.trgeo.2016.04.002.

Khan, M. I., Meguid, M. A., 2018. Experimental Investigation of the Shear Behavior of EPS Geofoam. International Journal of Geosynthetics and Ground Engineering 4(2), 12. https://doi.org/10.1007/s40891-018-0129-7.

Kim, H., Choi, B., Kim, J., 2010. Reduction of earth pressure on buried pipes by EPS geofoam inclusions. Geotech. Test J. 33(4), 304-313. https://doi.org/10.1520/GTJ102315.

Leshchinsky, B., Ling, H. I., 2013a. Numerical modeling of behavior of railway ballasted structure with geocell confinement. Geotext. Geomembranes 36, 33-43. https://doi.org/10.1016/j.geotexmem.2012.10.006

Leshchinsky, B., Ling, H. I., 2013b. Effects of Geocell Confinement on Strength and Deformation Behavior of Gravel. J. Geotech. Geoenvironmental Eng. 139(2). https://doi.org/10.1061/(ASCE)GT.1943-5606.0000757.

Ling, C., Ivens, J., Cardiff, P., Gilchrist, M. D., 2018. Deformation response of EPS foam under combined compression-shear loading. Part I: Experimental design and quasi-static tests. Int. J. Mech. Sci. 144, 480-489. https://doi.org/10.1016/j.ijmecsci.2018.06.014.

Liu, Y., Deng, A., Jaksa, M., 2019. Failure mechanisms of geocell walls and junctions. Geotext. Geomembranes 47(2), 104-120. https://doi.org/10.1016/j.geotexmem.2018.11.003.

Liyanapathirana, D. S., Ekanayake, S. D., 2016. Application of EPS geofoam in attenuating ground vibrations during vibratory pile driving. Geotext. Geomembranes 44(1), 59-69. https://doi.org/10.1016/j.geotexmem.2015.06.007.

Meguid, M. A., Ahmed, M. R., Hussein, M. G., Omeman, Z., 2017a. Earth pressure distribution on a rigid box covered with U-shaped geofoam wrap. International Journal of Geosynthetics and Ground Engineering 3(2), 11. https://doi.org/10.1007/s40891-017-0088-4.

Meguid, M. A., Hussein, M. G., Ahmed, M. R., Omeman, Z., Whalen, J., 2017b. Investigation of soil-geosynthetic-structure interaction associated with induced trench installation. Geotext. Geomembranes 45(4), 320-330. https://doi.org/10.1016/j.geotexmem.2017.04.004.

Mehrjardi, G. T., Motarjemi, F., 2018. Interfacial properties of Geocell-reinforced granular soils. Geotext. Geomembranes 46(4), 384-395. https://doi.org/10.1016/j.geotexmem.2018.03.002.

Mengelt, M., Edil, T. B., Benson, C. H., 2006. Resilient modulus and plastic deformation of soil confined in a geocell. Geosynth. Int. 13(5), 195-205. https://doi.org/10.1680/gein.2006.13.5.195.

Moghaddas Tafreshi, S. M., Khalaj, O., Dawson, A. R., 2014. Repeated loading of soil containing granulated rubber and multiple geocell layers. Geotext. Geomembranes 42(1), 25-38. https://doi.org/10.1016/j.geotexmem.2013.12.003.

Moghaddas Tafreshi, S. N., Dawson, A. R., 2012. A comparison of static and cyclic loading responses of foundations on geocell-reinforced sand. Geotext. Geomembranes 32, 55-68. https://doi.org/10.1016/j.geotexmem.2011.12.003.

Moghaddas Tafreshi, S. N., Khalaj, O., Dawson, A. R., 2013. Pilot-scale load tests of a combined multilayered geocell and rubber-reinforced foundation. Geosynth. Int. 20(3), 143-161. https://doi.org/10.1680/gein.13.00008.

Moghaddas Tafreshi, S.N., Rahimi, M., Dawson, A.R., Leshchinsky, B., 2018. Cyclic and Post-Cycling Anchor Response in Geocell-Reinforced Sand. Can. Geotech. J. https://doi.org/10.1139/cgj-2018-0559.

Mohajerani, A., Ashdown, M., Abdihashi, L., Nazem, M., 2017. Expanded polystyrene geofoam in pavement construction. Constr. Build. Mater. 157, 438-448. https://doi.org/10.1016/j.conbuildmat.2017.09.113.

Negussey, D., 2007. Design parameters for EPS geofoam. Soils Found. 47(1), 161-170. https://doi.org/10.3208/sandf.47.161.

Neto, J. A., 2019. Application of the two-layer system theory to calculate the settlements and vertical stress propagation in soil reinforcement with geocell. Geotext. Geomembranes 47(1), 32-41. https://doi.org/10.1016/j.geotexmem.2018.09.003.

Ngo, N. T., Indraratna, B., Rujikiatkamjorn, C., Mahdi Biabani, M., 2016. Experimental and discrete element modeling of geocell-stabilized subballast subjected to cyclic loading. J. Geotech. Geoenvironmental Eng. 142(4), 04015100. https://doi.org/10.1061/(ASCE)GT.1943-5606.0001431.

Ni, P., Mei, G., Zhao, Y., 2016. Displacement-dependent earth pressures on rigid retaining walls with compressible geofoam inclusions: physical modeling and analytical solutions. Int. J. Geomech. 17(6), 04016132.

Oliaei, M., Kouzegaran, S., 2017. Efficiency of cellular geosynthetics for foundation reinforcement. Geotext. Geomembranes 45(2), 11-22. https://doi.org/10.1016/j.geotexmem.2016.11.001.

Ossa, A., Romo, M. P., 2009. Micro-and macro-mechanical study of compressive behavior of expanded polystyrene geofoam. Geosynth. Int. 16(5), 327-338. https://doi.org/10.1680/gein.2009.16.5.327.

Ossa, A., Romo, M. P., 2012. Confining stress influence on EPS water absorption capability. Geotext. Geomembranes 35, 132-137. https://doi.org/10.1016/j.geotexmem.2012.03.003.

Ouria, A., Mahmoudi, A., 2018. Laboratory and numerical modeling of strip footing on geotextile-reinforced sand with cement-treated interface. Geotext. Geomembranes 46(1), 29-39. https://doi.org/10.1016/j.geotexmem.2017.09.003.

Özer, A. T., Akay, O., Fox, G. A., Bartlett, S. F., Arellano, D., 2014. A new method for remediation of sandy slopes susceptible to seepage flow using EPS-block geofoam. Geotext. Geomembranes 42(2), 166-180. https://doi.org/10.1016/j.geotexmem.2014.01.003.

Özer, A. T., 2016. Laboratory study on the use of EPS-block geofoam for embankment widening. Geosynth. Int. 23(2), 71-85. https://doi.org/10.1680/jgein.15.00033.

Palmeira, E. M., Antunes, L. G., 2010. Large scale tests on geosynthetic reinforced unpaved roads subjected to surface maintenance. Geotext. Geomembranes 28(6), 547-558. https://doi.org/10.1016/j.geotexmem.2010.03.002.

Piratheepan, J., Gnanendran, C.T. Arulrajah, A., 2012. Determination of c and φ from IDT and Unconfined Compression Testing and Numerical Analysis. J. Mater. Civil Eng. 24(9), 1153-1164.

Pokharel, S. K., Han, J., Leshchinsky, D., Parsons, R. L., 2018. Experimental evaluation of geocell-reinforced bases under repeated loading. Int. J. Pavement Res. and Technol. 11(2), 114-127. https://doi.org/10.1016/j.ijprt.2017.03.007.

Powell, W.D., Potter, J.F., Mayhew, H.C., Nunn, M.E., 1984. The structural design of bituminous roads, TRRL Report LR 1132, Crowthorne, UK.

Punetha, P., Nimbalkar, S., Khabbaz, H., 2019. Evaluation of additional confinement for three-dimensional geoinclusions under general stress state. Can. Geotech. J. https://doi.org/10.1139/cgj-2018-0866.

PRA (Public Roads Administration), 1992. Expanded Polystyrene Used in Road Embankments – Design, Construction and Quality Assurance. Form 482E. Public Roads Administration, Road Research Laboratory, Oslo, Norway

Pu, X., Shi, Z., Xiang, H., 2018. Feasibility of ambient vibration screening by periodic geofoam-filled trenches. Soil Dyn. Earthq. Eng. 104, 228-235. https://doi.org/10.1016/j.soildyn.2017.10.022.

Puppala, A. J., Ruttanaporamakul, P., Bheemasetti, T. V., Shafikhani, A., 2018. Laboratory and Field Investigations on Geofoam. J. Pipeline Syst. Eng. 10(1), 04018036.

Puppala, A. J., Ruttanaporamakul, P., Congress, S. S. C., 2019. Design and construction of lightweight EPS geofoam embedded geomaterial embankment system for control of settlements. Geotext. Geomembranes 47(3), 295-305. https://doi.org/10.1016/j.geotexmem.2019.01.015.

Rahimi, M., Moghaddas Tafreshi, S.N., Leshchinsky, B., 2018a. Assessing the Ultimate Uplift Capacity of Plate Anchors in Geocell-Reinforced Sand. Geosynth. Int. 25 (6), 612-629. https://doi.org/10.1680/jgein.18.00029.

Rahimi, M., Moghaddas Tafreshi, S.N., Leshchinsky, B., Dawson, A.R., 2018b. Experimental and Numerical Investigation of the Uplift Capacity of Plate Anchors in Geocell-Reinforced Sand. Geotext. Geomembranes 46 (6), 801–816. https://doi.org/10.1016/j.geotexmem.2018.07.010.

Rahman, M. A., Imteaz, M. A., Arulrajah, A., Piratheepan, J., Disfani, M. M., 2015. Recycled construction and demolition materials in permeable pavement systems: geotechnical and hydraulic characteristics. J. Clean Prod. 90, 183-194. https://doi.org/10.1016/j.jclepro.2014.11.042.

Satyal, S. R., Leshchinsky, B., Han, J., Neupane, M., 2018. Use of cellular confinement for improved railway performance on soft subgrades. Geotext. Geomembranes 46(2), 190-205. https://doi.org/10.1016/j.geotexmem.2017.11.006.

Selvakumar, S., Soundara, B., 2019. Swelling behaviour of expansive soils with recycled geofoam granules column inclusion. Geotext. Geomembranes 47(1), 1-11. https://doi.org/10.1016/j.geotexmem.2018.08.007.

Shafikhani, A., Bheemasetti, T. V., Puppala, A. J., 2017. Effect of Seasonal Changes on a Hybrid Soil–Geofoam Embankment System. International Journal of Geosynthetics and Ground Engineering 3(4), 39. https://doi.org/10.1007/s40891-017-0116-4.

Simulia, A. V., 2013. ABAQUS 6.13 User's manual. Dassault Systems, Providence, RI.

Sireesh, S., Sitharam, T. G., Dash, S. K., 2009. Bearing capacity of circular footing on geocell–sand mattress overlying clay bed with void. Geotext. Geomembranes 27(2), 89-98. https://doi.org/10.1016/j.geotexmem.2008.09.005.

Sitharam, T. G., Hegde, A., 2013. Design and construction of geocell foundation to support the embankment on settled red mud. Geotext. Geomembranes 41, 55-63. https://doi.org/10.1016/j.geotexmem.2013.08.005.

Song, F., Liu, H., Ma, L., Hu, H., 2018. Numerical analysis of geocell-reinforced retaining wall failure modes. Geotext. Geomembranes 46(3), 284-296. https://doi.org/10.1016/j.geotexmem.2018.01.004.

Song, F., Liu, H., Yang, B., Zhao, J., 2019. Large-scale triaxial compression tests of geocell-reinforced sand. Geosynth. Int, 1-29. https://doi.org/10.1680/jgein.19.00019.

Stark, T. D., Arellano, D., Horvath, J. S., Leshchinsky, D., 2004. Geofoam applications in the design and construction of highway embankments (No. NCHRP Project 24-11). Transportation Research Board, Washington, D.C.

Stark, T. D., Bartlett, S. F., Arellano, D., 2012. Expanded polystyrene (EPS) geofoam applications and technical data. The EPS Industry Alliance, 1298, 36.

Suku, L., Prabhu, S. S., Ramesh, P., Babu, G. S., 2016. Behavior of geocell-reinforced granular base under repeated loading. Transp. Geotech. 9, 17-30. https://doi.org/10.1016/j.trgeo.2016.06.002.

Sun, X., Han, J., Kwon, J., Parsons, R. L., Wayne, M. H., 2015. Radial stresses and resilient deformations of geogrid-stabilized unpaved roads under cyclic plate loading tests. Geotext. Geomembranes 43(5), 440-449. https://doi.org/10.1016/j.geotexmem.2015.04.018.

Tavakoli Mehrjardi, G., Moghaddas Tafreshi, S. N., Dawson, A. R., 2012. Combined use of geocell reinforcement and rubber–soil mixtures to improve performance of buried pipes. Geotext. Geomembranes 34, 116-130. https://doi.org/10.1016/j.geotexmem.2012.05.004.

Tavakoli Mehrjardi, G. H., Motarjemi, F., 2018. Interfacial properties of Geocell-reinforced granular soils. Geotext. Geomembranes 46(4), 384-395. https://doi.org/10.1016/j.geotexmem.2018.03.002.

Tavakoli Mehrjardi, G., Behrad, R., Moghaddas Tafreshi, S. N., 2019. Scale effect on the behavior of geocell-reinforced soil. Geotext. Geomembranes 47(2), 154-163. https://doi.org/10.1016/j.geotexmem.2018.12.003.

Tavira, J., Jiménez, J.R., Ayuso, J., Sierra, M.J., Ledesma, E.F., 2018. Functional and structural parameters of a paved road section constructed with mixed recycled aggregates from non-selected construction and demolition waste with excavation soil. Constr. Build. Mater. 164, 57-69. https://doi.org/10.1016/j.conbuildmat.2017.12.195.

Tanyu, B. F., Aydilek, A. H., Lau, A. W., Edil, T. B., Benson, C. H., 2013. Laboratory evaluation of geocell-reinforced gravel subbase over poor subgrades. Geosynth. Int. 20(2), 47-61. https://doi.org/10.1680/gein.13.00001.

Thakur, J. K., Han, J., Pokharel, S. K., Parsons, R. L., 2012. Performance of geocell-reinforced recycled asphalt pavement (RAP) bases over weak subgrade under cyclic plate loading. Geotext. Geomembranes 35, 14-24. https://doi.org/10.1016/j.geotexmem.2012.06.004.

Thakur, J. K., 2013. Geocell-reinforced unpaved and paved roads with recycled asphalt pavement (RAP) bases: experimental study and damage model development (Doctoral dissertation, University of Kansas).

Thakur, J. K., Han, J., Parsons, R. L., 2016. Factors influencing deformations of geocell-reinforced recycled asphalt pavement bases under cyclic loading. J. Mater. Civil Eng. 29(3), 04016240.

Trandafir, A. C., Bartlett, S. F., Lingwall, B. N., 2010. Behavior of EPS geofoam in stress-controlled cyclic uniaxial tests. Geotext. Geomembranes 28(6), 514-524. https://doi.org/10.1016/j.geotexmem.2010.01.002.

Trandafir, A. C., Erickson, B. A., 2011. Stiffness degradation and yielding of EPS geofoam under cyclic loading. J. Mater. Civil Eng. 24(1), 119-124.

Vahedifard, F., Shahrokhabadi, S., Leshchinsky, D., 2016. Geosynthetic-reinforced soil structures with concave facing profile. Geotext. Geomembranes 44 (3), 358-365.

Venkateswarlu, H., Ujjawal, K. N., Hegde, A., 2018. Laboratory and numerical investigation of machine foundations reinforced with geogrids and geocells. Geotext. Geomembranes 46(6), 882-896. https://doi.org/10.1016/j.geotexmem.2018.08.006.

Wesseloo, J., Visser, A. T., Rust, E., 2009. The stress–strain behaviour of multiple cell geocell packs. Geotext. Geomembranes 27(1), 31-38. https://doi.org/10.1016/j.geotexmem.2008.05.009.

Witthoeft, A. F., Kim, H., 2016. Numerical investigation of earth pressure reduction on buried pipes using EPS geofoam compressible inclusions. Geosynth Int. 23(4), 1-14. https://doi.org/10.1680/jgein.15.00054.

Yang, X., 2010. Numerical analyses of geocell-reinforced granular soils under static and repeated loads (Doctoral dissertation, University of Kansas).

Yang, X., Han, J., Parsons, R. L., Leshchinsky, D., 2010. Three-dimensional numerical modeling of single geocell-reinforced sand. Frontiers of Architecture and Civil Engineering in China, 4(2), 233-240. https://doi.org/10.1007/s11709-010-0020-7.

Yang, X., Han, J., Pokharel, S. K., Manandhar, C., Parsons, R. L., Leshchinsky, D., Halahmi, I., 2012. Accelerated pavement testing of unpaved roads with geocell-reinforced sand bases. Geotext. Geomembranes 32, 95-103. https://doi.org/10.1016/j.geotexmem.2011.10.004.

Zhang, L., Zhao, M., Shi, C., Zhao, H., 2010. Bearing capacity of geocell reinforcement in embankment engineering. Geotext. Geomembranes 28(5), 475-482. https://doi.org/10.1016/j.geotexmem.2009.12.011.

Zou, Y., Leo, C. J., Small, J. C., 2000. Behaviour of EPS Geofoam as Flexible Pavement Subgrade Material in Model Tests. Geosynth. Int. 7(1), 1-22. https://doi.org/10.1680/gein.7.0163.

List of Figures

Fig. 1	(a) Schematic view of the possible failure mechanism for unreinforced pavement foundation, (b) typical punching failure of EPS geofoam, (c) Schematic view of the possible failure mechanism of geocell reinforced pavement foundations (d) typical wider deformation basin of EPS geofoam under geocell reinforced pavement foundation
Fig. 2	Gradation diagram of soil used in the backfill - based on ASTM D 2487-11 (Ghotbi Siabil et al., 2019)
Fig. 3	(a) Schematic view of the testing apparatus (not to scale) and test parameters (units in mm), modified after Ghotbi Siabil et al., 2019 for geocell reinforcement (b) Schematic illustration of loading pattern including: stage 1, including 100 repetitions of 275 kPa cyclic pressure and stage 2, including 400 repetitions of 550 kPa cyclic pressure
Fig. 4	(a) Placement of EPS geofoam blocks inside test box, (b) Preparation of geocell-reinforced mattress and, (c) Completed test installation prior to loading including reaction beam, loading plate, hydraulic jack, load cell and LVDTs (modified after Ghotbi Siabil et al., 2019; for geocell reinforcement)
Fig. 5	Typical variation in the settlement of loading surface with load cycles for (a) unreinforced and (b) reinforced installations. Typical variation of the transferred pressure on top of EPS geofoam bed with load cycles for (c) unreinforced and (d) reinforced installations. The thickness of soil layer placed on EPS 30/20 was 400 mm
Fig. 6	Distribution of pressure in depth of EPS geofoam layers for unreinforced and reinforced pavements at applied pressure of (a) 275 kPa and (b) 550 kPa – the highlighted regions in gray and green colors indicate stable cyclic pressure thresholds for EPS 30 and EPS 20
Fig. 7	Variation of (a) peak settlements of the loading surface, (b) permanent settlements of the loading surface (c) peak transferred pressure on top of EPS geofoam bed, with number of loading cycles for unreinforced and geocell-reinforced pavement foundations of different soil thicknesses
Fig. 8	Variation of improvement factors with soil thickness at the first and last cycle of each loading stages: (a) IF for peak surface settlement, (b) IF for permanent or residual surface settlement, (c) IF for the transferred pressure on EPS
Fig. 9	Peak deflection basin of the pavement surface for reinforced and unreinforced pavement foundations on EPS 30/20 with three thicknesses of 400, 500 and 600 mm after 500 total load repetitions
Fig. 10	Variation of (a) peak settlements of the loading surface, (b) permanent (residual) settlements of the loading surface, (c) peak transferred pressure on top of EPS geofoam bed, with number of loading cycles for unreinforced and geocell-reinforced pavement foundations of different EPS densities
Fig. 11	Variation of (a) peak settlements of the loading surface, (b) permanent (residual) settlements of the loading surface, (b) peak transferred pressure on top of EPS 20/20 geofoam bed, with number of loading cycles for unreinforced and geocell-reinforced pavement foundations of different soil thicknesses
Fig. 12	(a) Total assembly of the full numerical model including: loading plate, geocell mattress, soil layer, upper and bottom EPS layers, (b) Finite element mesh of the whole model, (c) Finite element mesh of geocell, (d) one-time static loading used in the numerical analyses.
Fig. 13	Numerical and experimental result for the settlement of the (a) unreinforced and (b) geocell-reinforced pavement surface with different soil thickness after application of the first cycle of 275 kPa and 550 kPa loads. Numerical and experimental result for the transferred pressure on the top of upper EPS layer for (c) unreinforced and (d) geocell-reinforced pavements with different soil thickness after application of the first cycle of 275 kPa and 550 kPa loads
Fig. 14	Settlement of pavement surface, upper EPS layer (EPS 30) and bottom EPS layer (EPS 20) of reinforced and unreinforced pavements for the applied load of 550 kPa
Fig. 15	Longitudinal strain in geocell of reinforced pavements with soil thickness of 600 mm on: (a): EPS 20/20, (b) EPS 30/20 for the applied pressure of 550 kPa

List of Tables

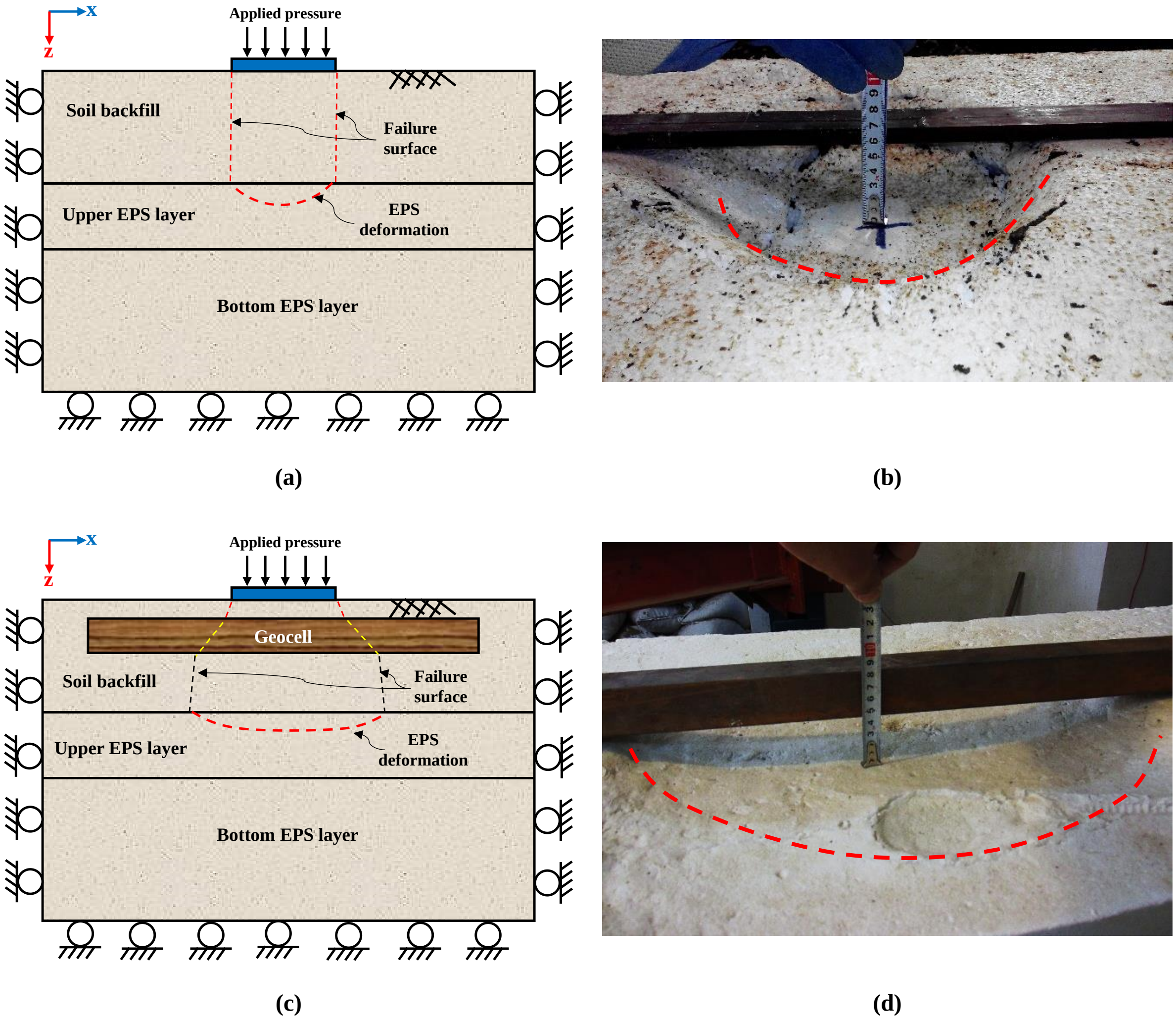

Fig. 1. (a) Schematic view of the possible failure mechanism for unreinforced pavement foundation, (b) typical punching failure of EPS geofoam, (c) Schematic view of the possible failure mechanism of geocell reinforced pavement foundations (d) typical wider deformation basin of EPS geofoam under geocell reinforced pavement foundation

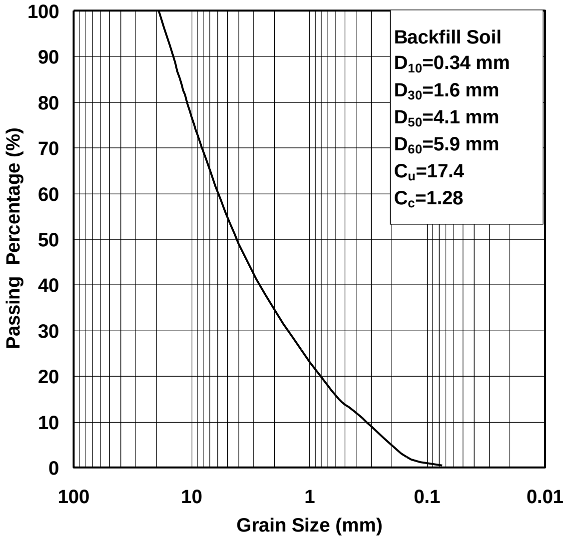

Fig. 2. Gradation diagram of soil used in the backfill - based on ASTM D 2487-11 (Ghotbi Siabil et al., 2019)

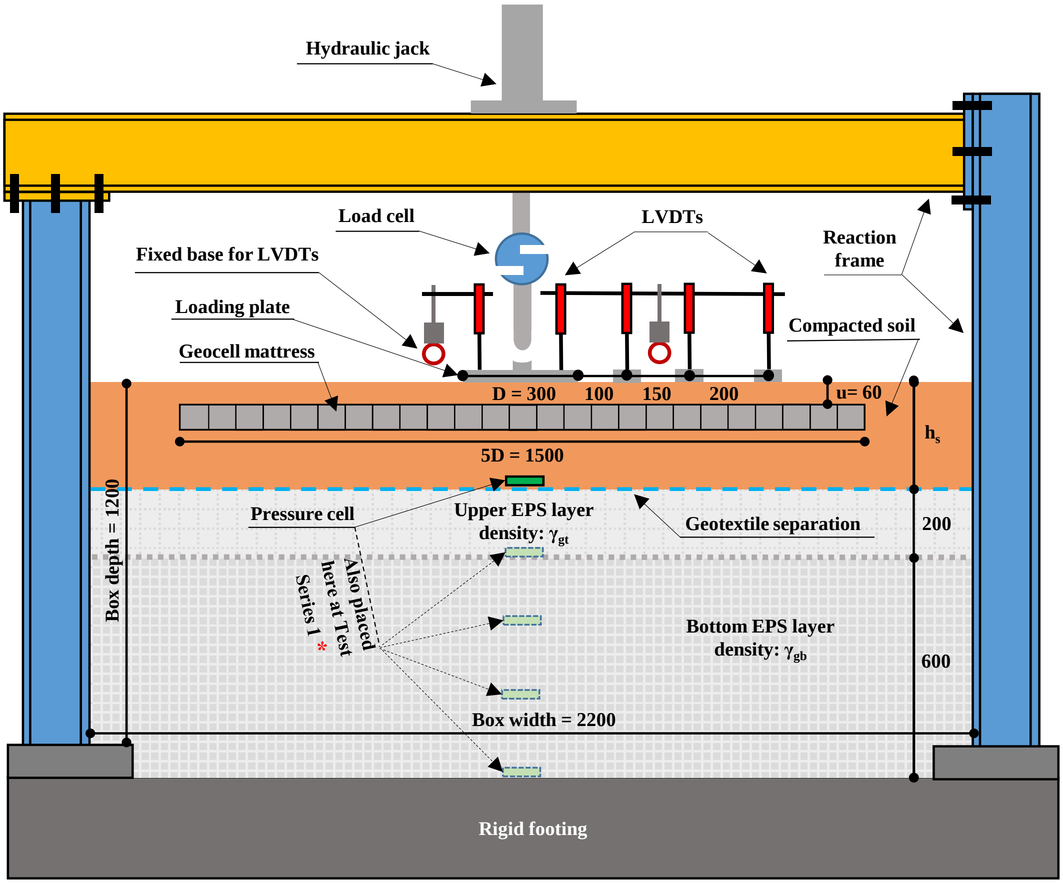

** With only one available earth pressure cell, one test was replicated 5 times in separate installations, placing the earth pressure cell at depths 0, 200, 400, 600 and 800 mm from top of EPS surface*

(a)

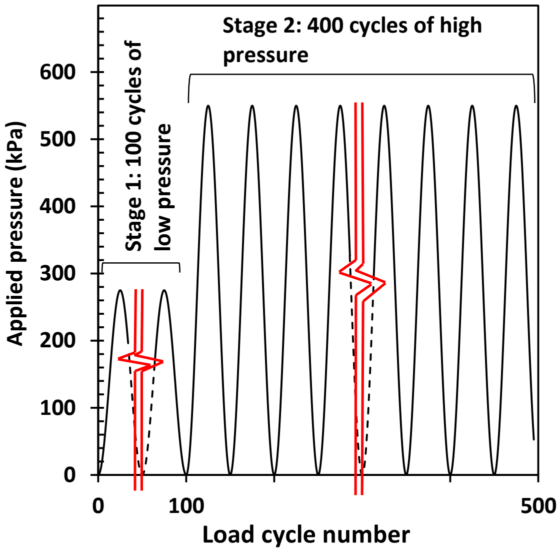

(b)

Fig. 3. (a) Schematic view of the testing apparatus (not to scale) and test parameters (units in mm), modified after Ghotbi Siabil et al., 2019 for geocell reinforcement (b) Schematic illustration of loading pattern including: stage 1, including 100 repetitions of 275 kPa cyclic pressure and stage 2, including 400 repetitions of 550 kPa cyclic pressure.

(a) **(b)**

(c)

Fig. 4. (a) Placement of EPS geofoam blocks inside test box, (b) Preparation of geocell-reinforced mattress and, (c) Completed test installation prior to loading including reaction beam, loading plate, hydraulic jack, load cell and LVDTs (modified after Ghotbi Siabil et al., 2019; for geocell reinforcement).

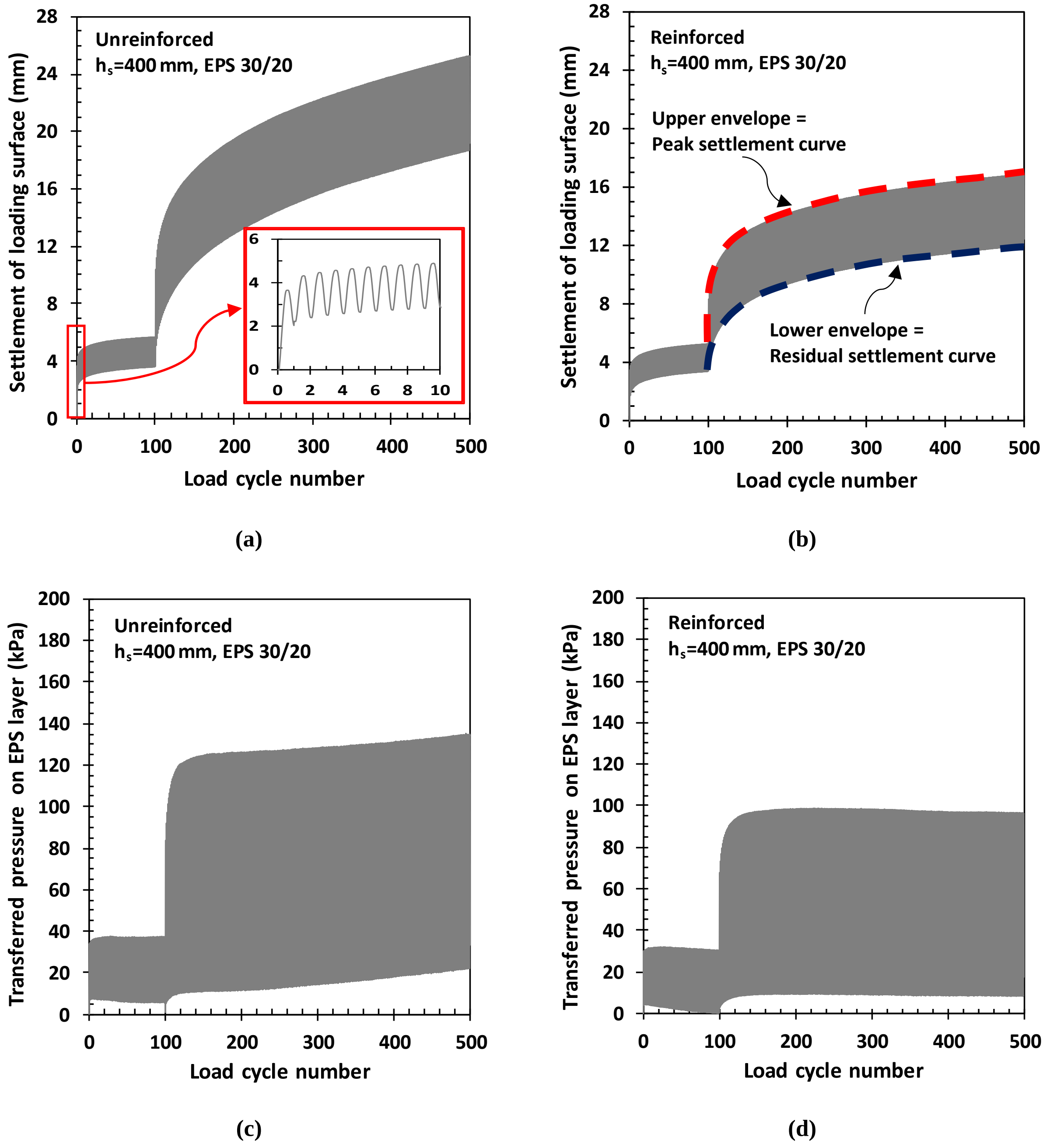

Fig. 5. Typical variation in the settlement of loading surface with load cycles for (a) unreinforced and (b) reinforced installations. Typical variation of the transferred pressure on top of EPS geofoam bed with load cycles for (c) unreinforced and (d) reinforced installations. The thickness of soil layer placed on EPS 30/20 was 400 mm.

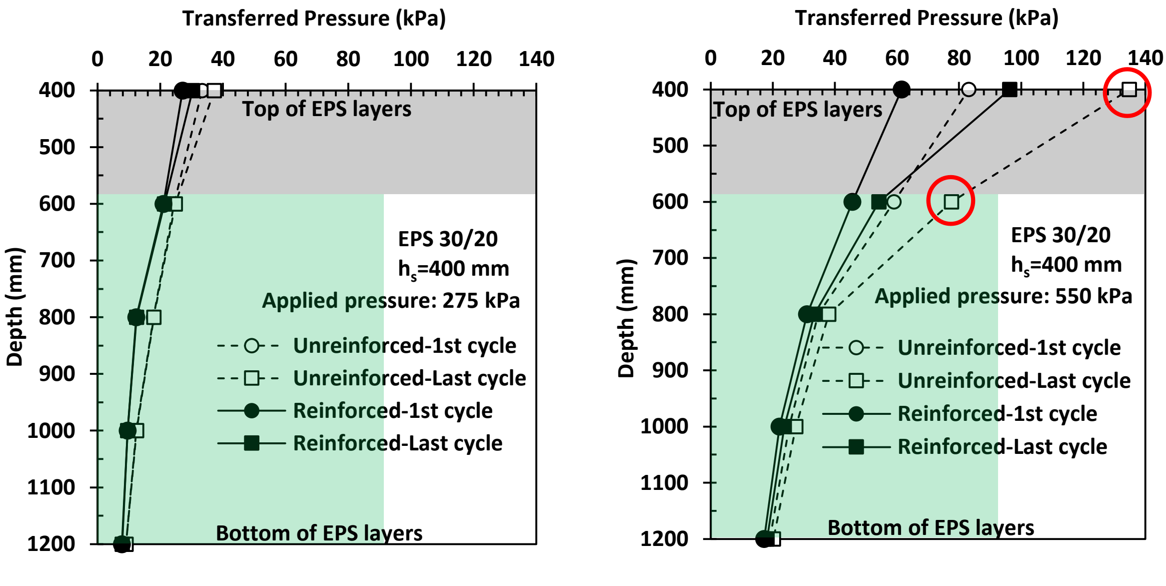

(a) (b)

Fig. 6. Distribution of pressure in depth of EPS geofoam layers for unreinforced and reinforced pavements at applied pressure of (a) 275 kPa and (b) 550 kPa – the highlighted regions in gray and green colors indicate stable cyclic pressure thresholds for EPS 30 and EPS 20

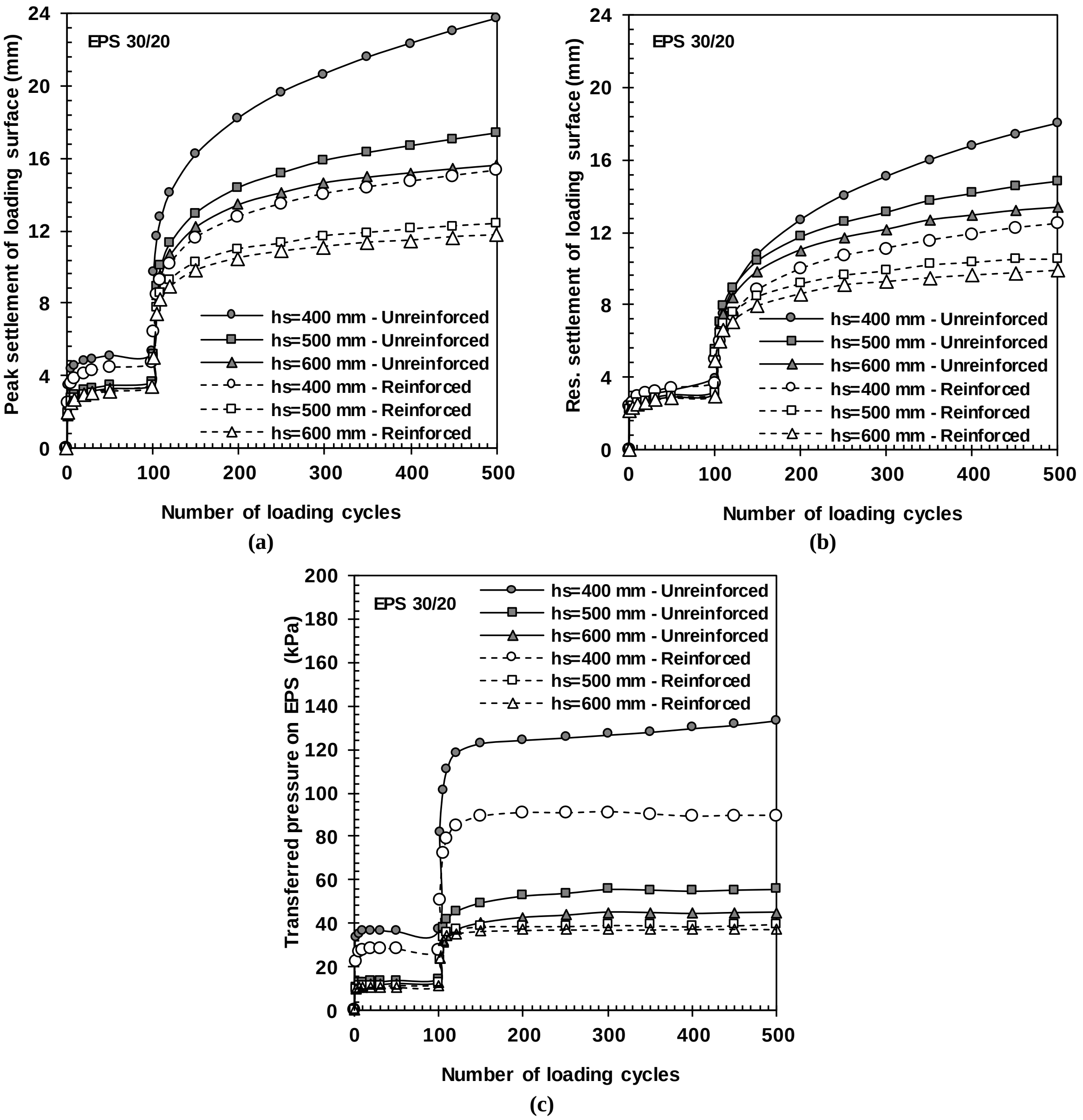

Fig. 7. Variation of (a) peak settlements of the loading surface, (b) permanent settlements of the loading surface (c) peak transferred pressure on top of EPS geofoam bed, with number of loading cycles for unreinforced and geocell-reinforced pavement foundations of different soil thicknesses

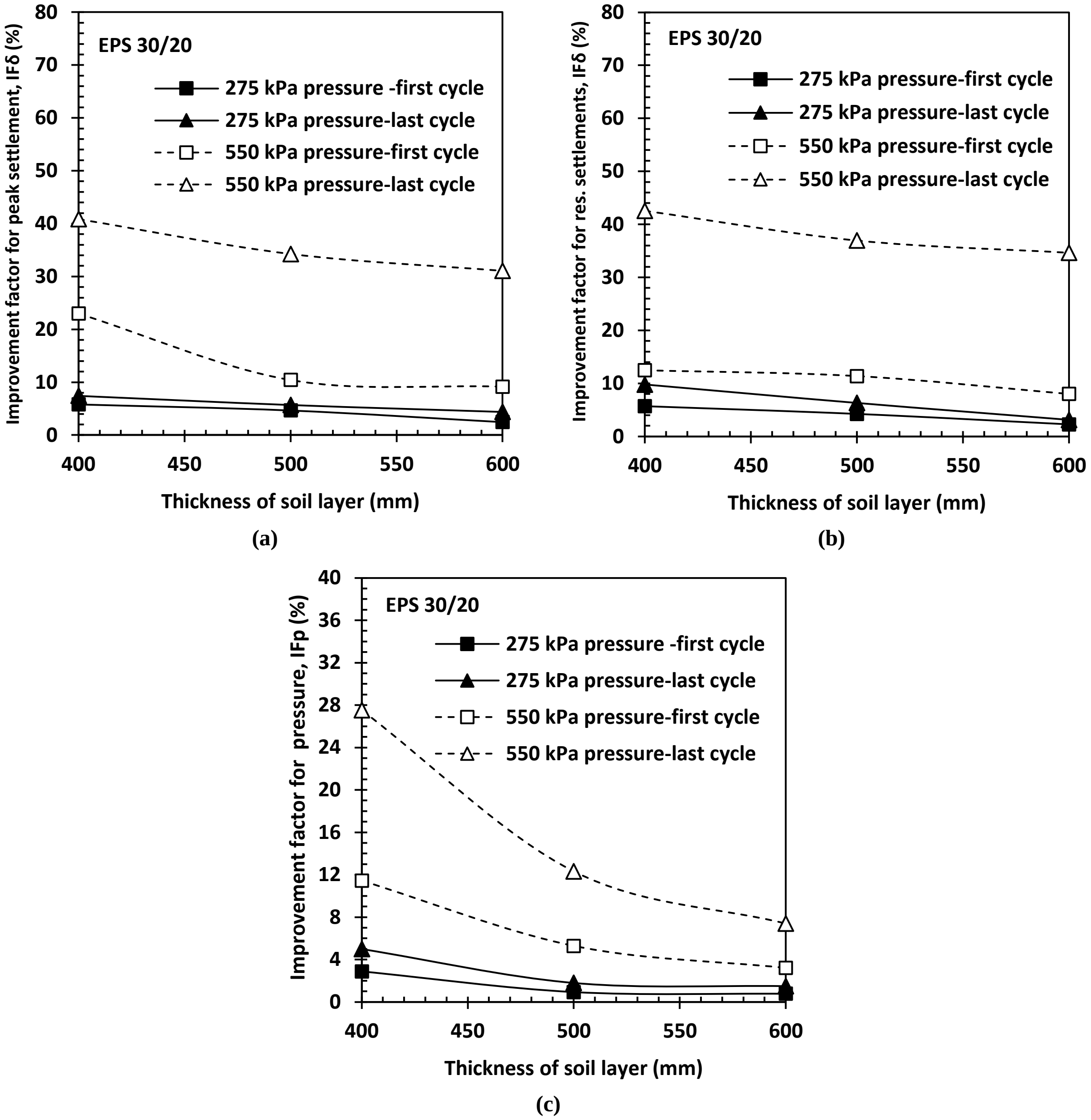

Fig. 8. Variation of improvement factors with soil thickness at the first and last cycle of each loading stages: (a) IF for peak surface settlement, (b) IF for permanent or residual surface settlement, (c) IF for the transferred pressure on EPS.

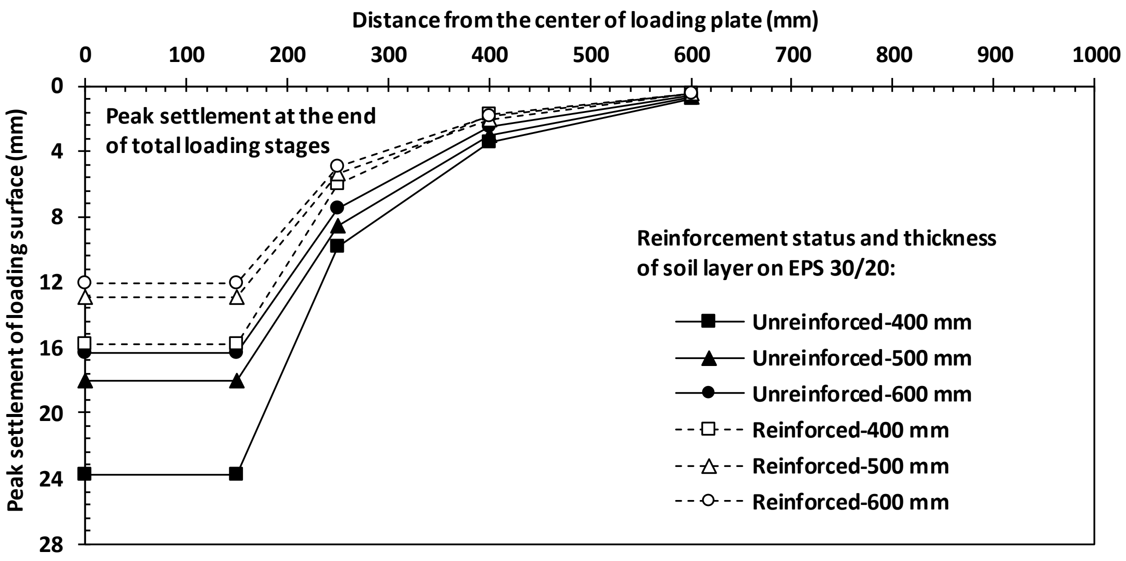

Fig. 9. Peak deflection basin of the pavement surface for reinforced and unreinforced pavement foundations on EPS 30/20 with three thicknesses of 400, 500 and 600 mm after 500 total load repetitions

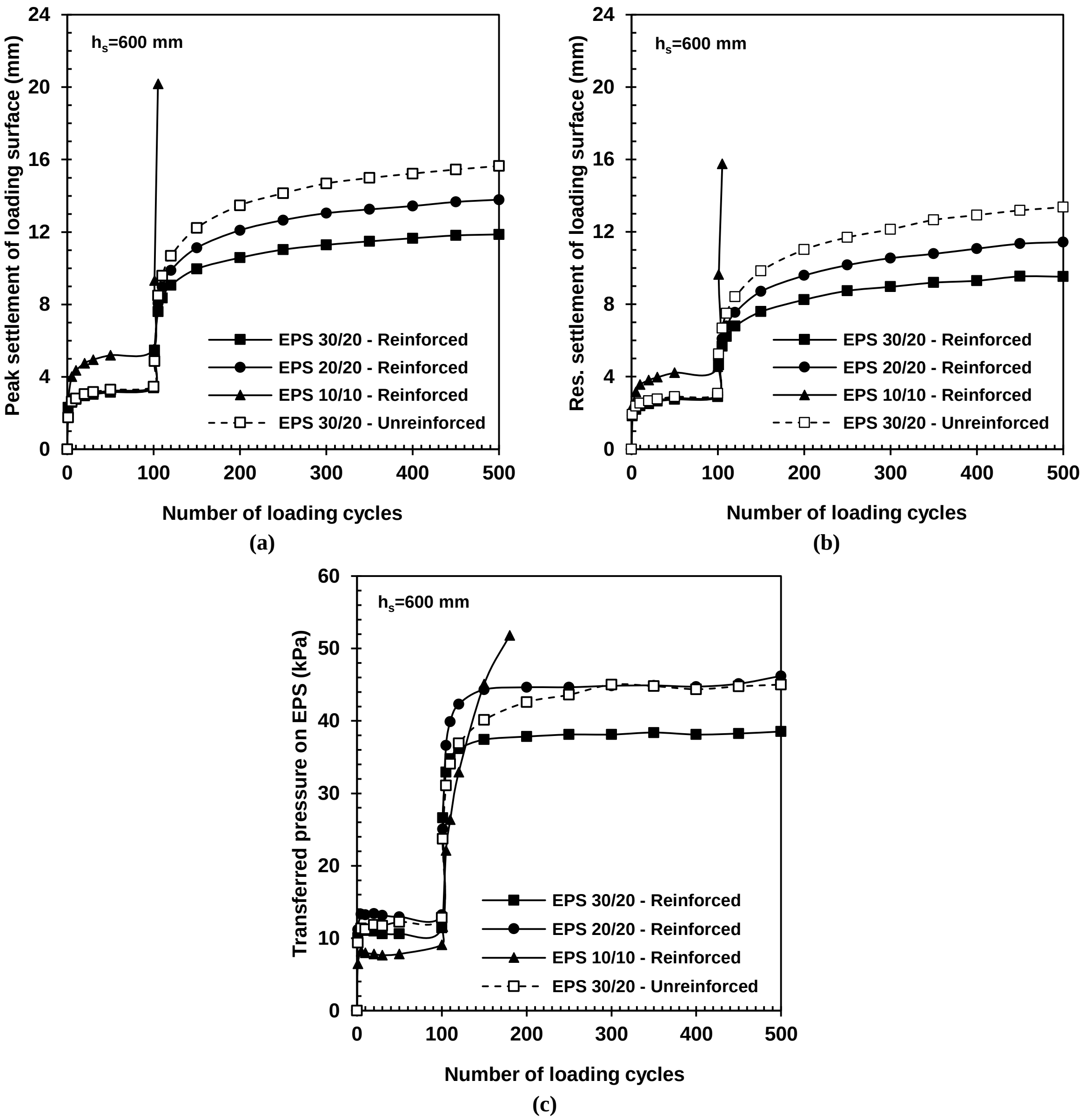

Fig. 10. Variation of (a) peak settlements of the loading surface, (b) permanent (residual) settlements of the loading surface, (c) peak transferred pressure on top of EPS geofoam bed, with number of loading cycles for unreinforced and geocell-reinforced pavement foundations of different EPS densities

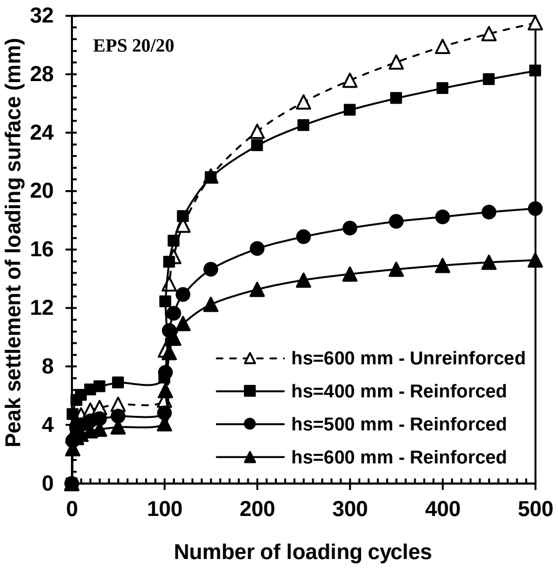

(a)

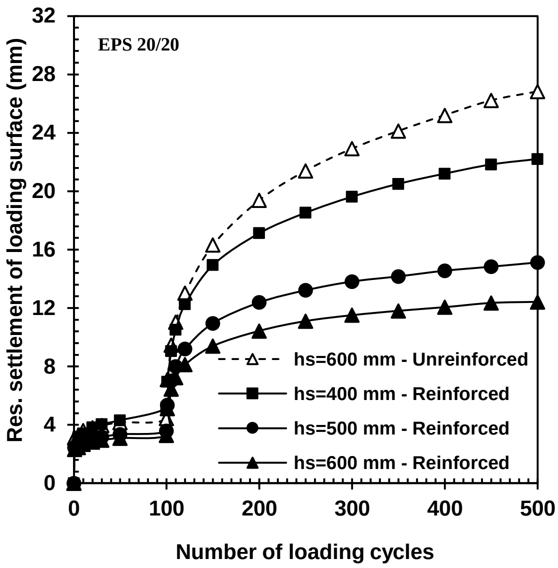

(b)

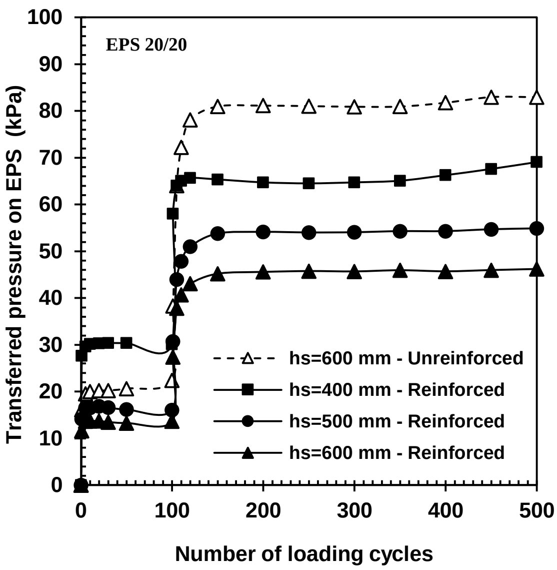

(c)

Fig. 11. Variation of (a) peak settlements of the loading surface, (b) permanent (residual) settlements of the loading surface, (b) peak transferred pressure on top of EPS 20/20 geofoam bed, with number of loading cycles for unreinforced and geocell-reinforced pavement foundations of different soil thicknesses

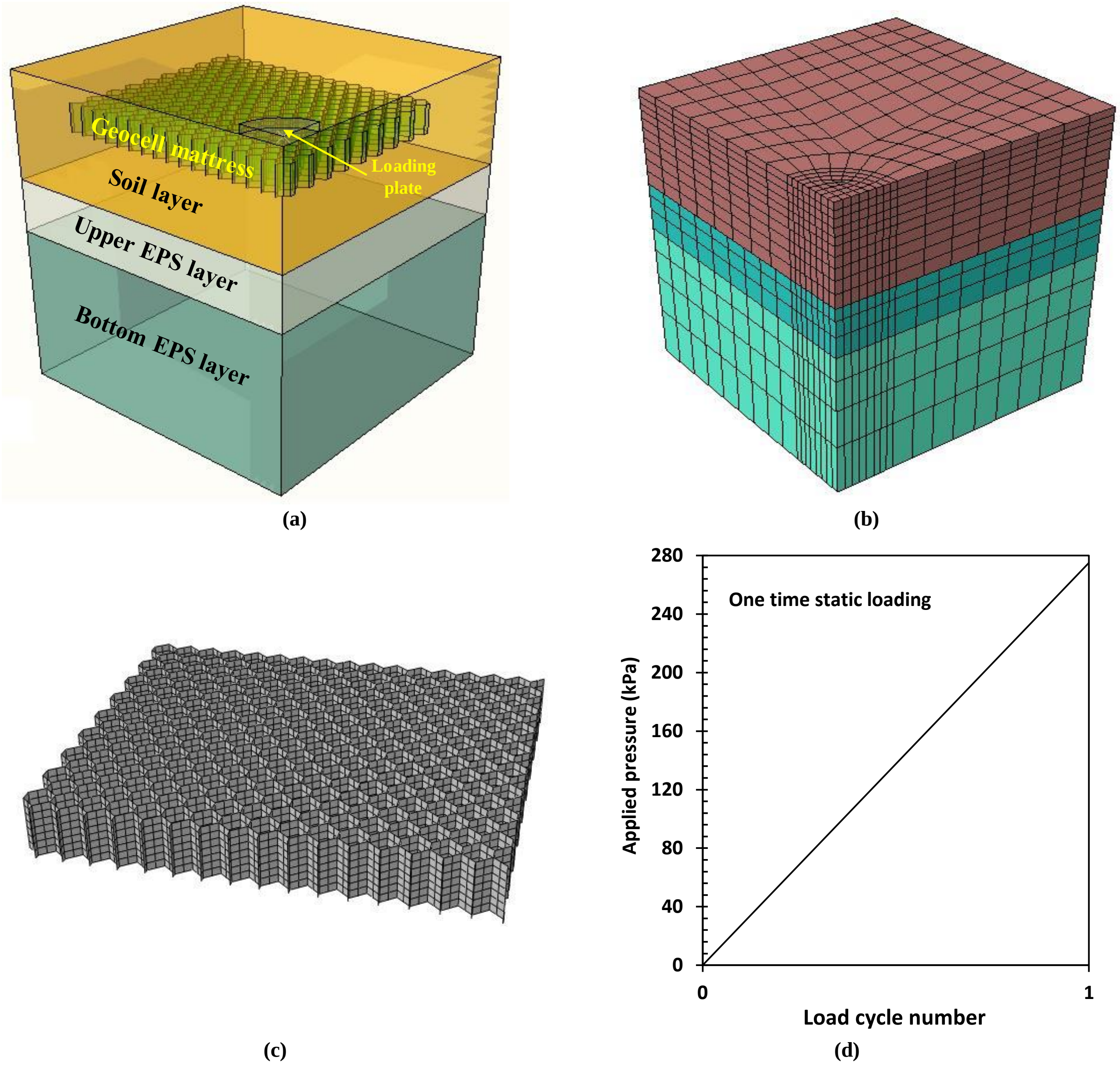

Fig. 12. (a) Total assembly of the full numerical model including: loading plate, geocell mattress, soil layer, upper and bottom EPS layers, (b) Finite element mesh of the whole model, (c) Finite element mesh of geocell, (d) one-time static loading used in the numerical analyses.

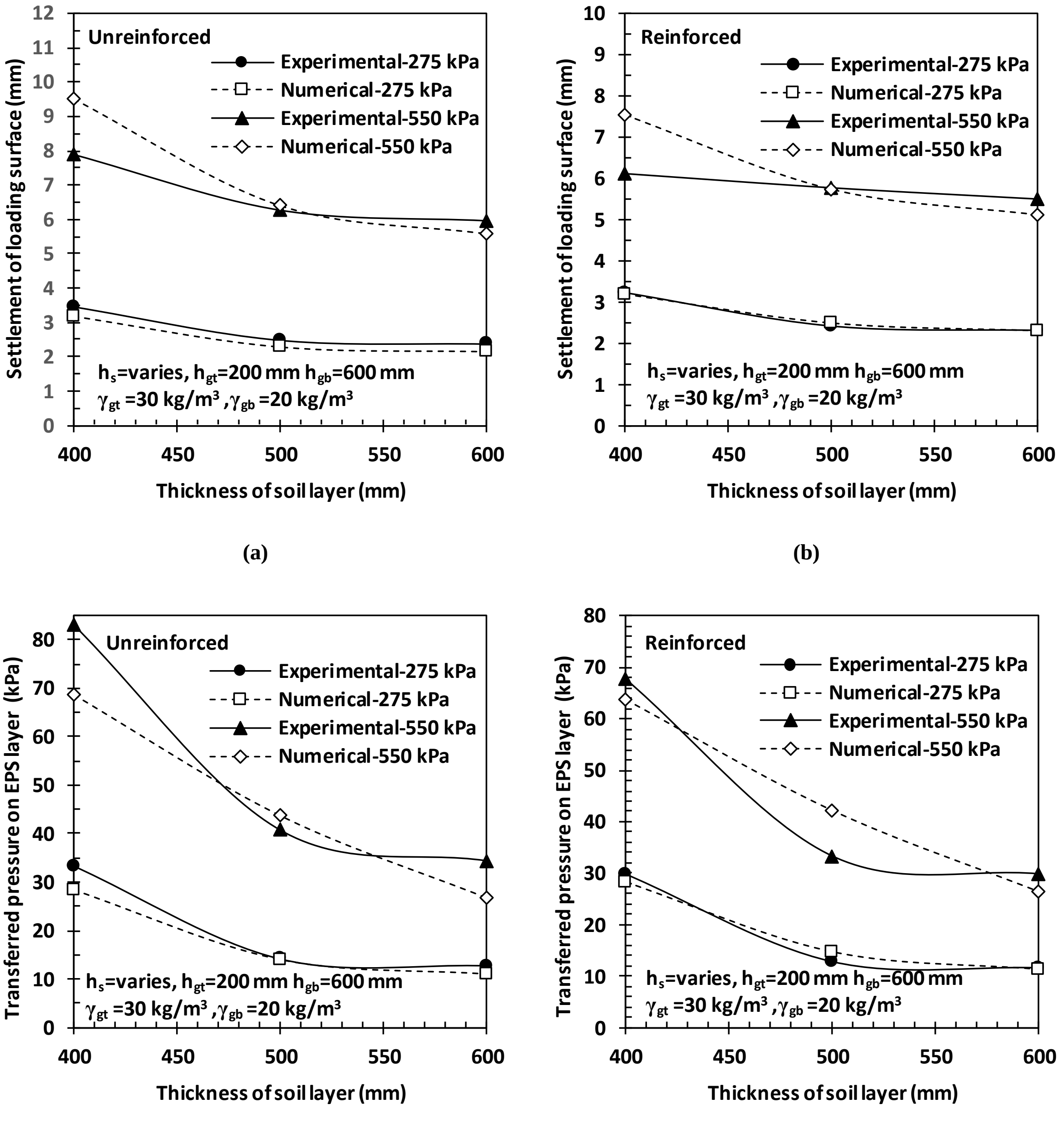

Fig. 13. Numerical and experimental result for the settlement of the (a) unreinforced and (b) geocell-reinforced pavement surface with different soil thickness after application of the first cycle of 275 kPa and 550 kPa loads. Numerical and experimental result for the transferred pressure on the top of upper EPS layer for (c) unreinforced and (d) geocell-reinforced pavements with different soil thickness after application of the first cycle of 275 kPa and 550 kPa loads.

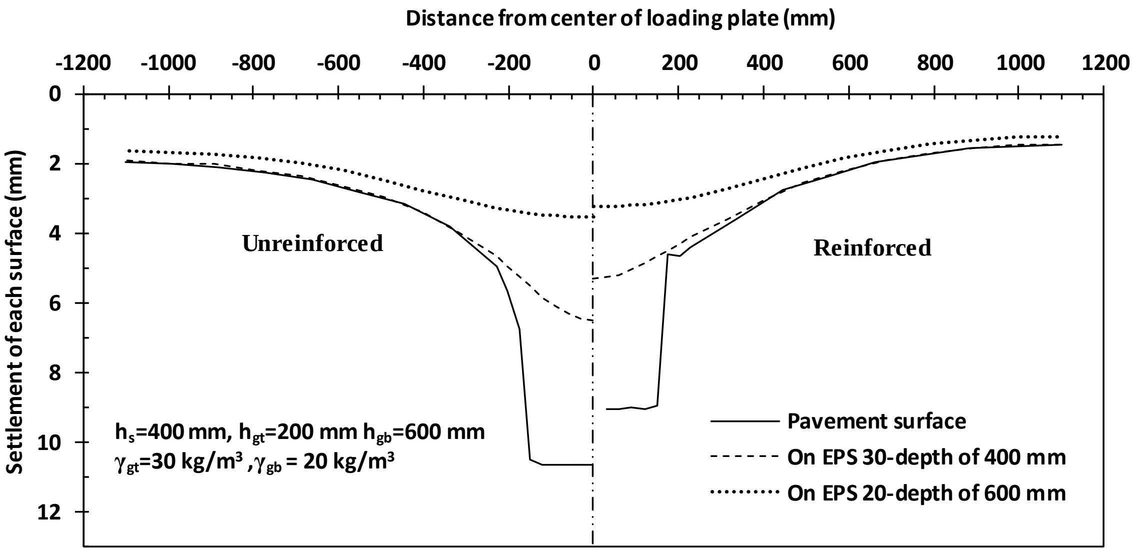

(a)

Fig. 14. Settlement of pavement surface, upper EPS layer (EPS 30) and bottom EPS layer (EPS 20) of reinforced and unreinforced pavements for the applied load of 550 kPa.

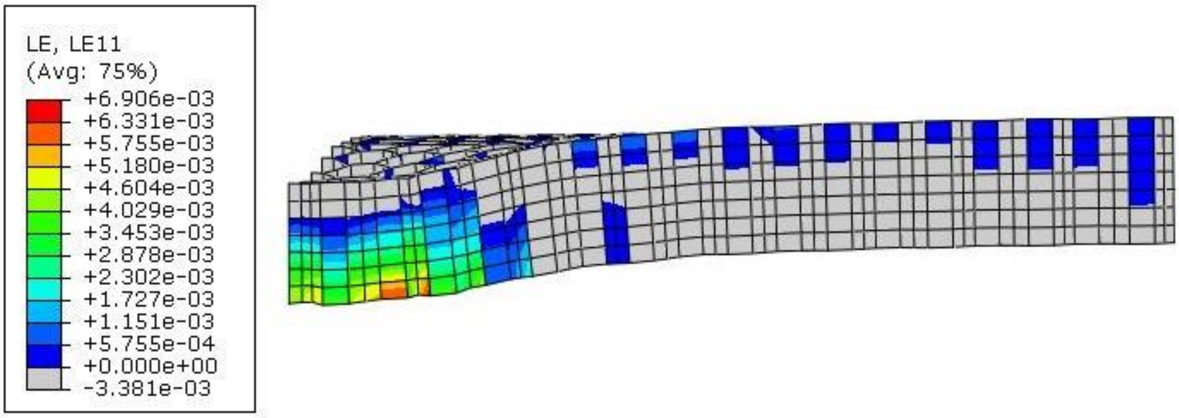

(a)

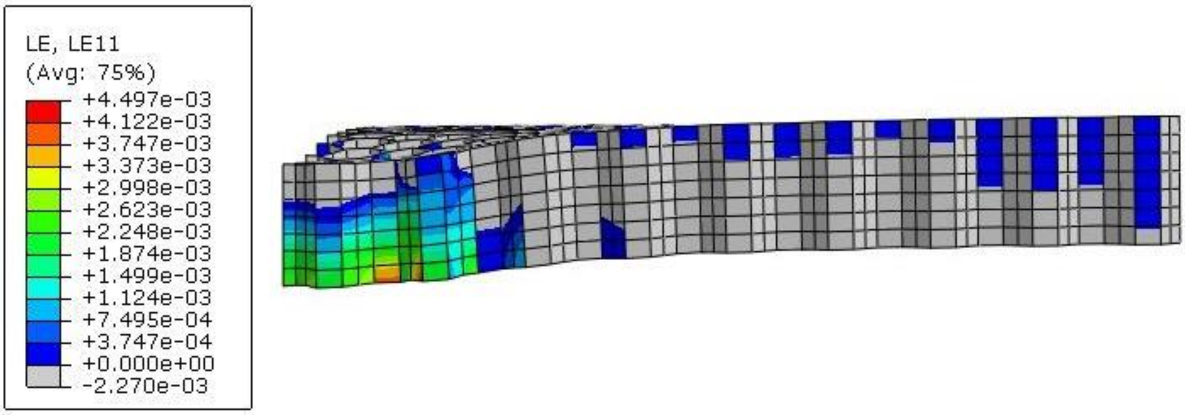

(b)

Fig. 15. Longitudinal strain in geocell of reinforced pavements with soil thickness of 600 mm on: (a): EPS 20/20, (b) EPS 30/20 for the applied pressure of 550 kPa.

Table 1.

Physical and mechanical properties of EPS geofoam (Ghotbi Siabil et al., 2019)

Engineering properties	EPS 10	EPS 20	EPS 30
Measured density (kg/m^3)	8.5~9.5	17~19	27~29
Angle of internal friction (º)	~1	~ 2	~ 3
Apparent cohesion (kPa)	~20	~40	~70
Elastic modulus - 1% strain (MPa)	0.37	0.81	2.16
Compressive strength - 10% strain (kPa)	39.3	83.67	156.4
Resilient modulus - 0.1 Hz loading (MPa)	2.4	4.1	5.5
Stable threshold of cyclic stress - P_s (kPa)	~40	~90	~140

Table 2.

The engineering characteristics of geocell reinforcement and geotextile separation (after Ghotbi Siabil et al., 2019)

Property	Geocell reinforcements	Geotextile separation
Type of geotextile	Non-woven	Non-woven
Material	Polypropylene	Polypropylene
Mass per unit area (gr/m^2)	190	170
Tensile strength (MD), kN/m	13.1	16
Tensile strength (CMD), kN/m	13.1	18
Elongation at maximum load, %	-	>50
Static puncture (CBR), kN	-	2.7
Thickness under 2 kN/m^2 (mm)	0.57	-
Thickness under 200 kN/m^2 (mm)	0.47	-
Strength at 5% (kN/m)	5.7	-
Effective opening size (mm)	0.08	-

Table 3.

Test program for large cyclic plate load experiments

Test Series		h_s (mm)	γ_{gt} (kg/m^3)	γ_{gb} (kg/m^3)	Reinforcement	No. of tests	Purpose of the test
1		400	30	20	No	10*+5***	Effect of reinforcement on pressure distribution in EPS layers
					Yes		
2	**a**	400**	30	20	No	2+4***	Effect of unreinforced soil thickness over EPS 30/20 on pavement response
	b	500					
	c	600					
	d	400**	30	20	Yes	2+4***	Effect of reinforced soil thickness over EPS 30/20 on pavement response
	e	500					
	f	600					
3	**a**	400	20	20	Yes	3+4***	Effect of reinforced soil thickness over EPS 20/20 on pavement response
	b	500					
	c	600					
4		600	20	20	No	1+1***	Effect of unreinforced soil thickness over EPS 20/20 on pavement response
5		600	10	10	Yes	1+1***	Effect of lower EPS density with higher soil thickness on pavement response

** Due to insufficient number of available pressure cells, one test was repeated 5 times with placing the pressure sensor at the indicated depths (0, 200, 400, 600 and 800 mm from top of EPS surface in separate tests)*

*** Indicates the tests which have been previously performed in Test Series 1*

**** Indicates the number of tests which have been repeated two or three times to ensure the accuracy of the test data. For example, in test Series 3, total of 7 tests were performed, including 3 independent tests plus 4 replicates.*

Note: dry density of soil layers varies from 18.7 to 19.6 (kN/m^3) from bottom to top of soil cover

Table 4.

Resilient modulus for different soil thicknesses under 275 and 550 kPa pressures for pavement foundations including EPS 30/20

Applied pressure (kPa)	Soil thickness (mm)	Unreinforced M_r (MPa)		Reinforced M_r (MPa)	
		Initial value	Stabilized value	Initial value	Stabilized value
275	400	39.3	32.3	39.4	36.2
	500	99.9	74.9	99.0	84.5
	600	104.4	79.0	104.6	90.6
550	400	20.7	14.4	29.4	22.0
	500	26.5	17.3	29.3	23.2
	600	28.9	19.0	32.1	23.6

Table 5.

Improvement factors of 600 mm thick reinforced pavement foundations on EPS 30/20, EPS 20/20 and EPS 10/10 compared to unreinforced EPS 30/20

Type of Settlement	IFδ (reinforced compared with unreinforced case)				IFp (reinforced compared with unreinforced case)			
	First loading stage (Pm = 275 kPa)		Second loading stage (Pm =550 kPa)		First loading stage (Pm = 275 kPa)		Second loading stage (Pm =550 kPa)	
	$IF\delta_{1,1}$	$IF\delta_{1,100}$	$IF\delta_{2,1}$	$IF\delta_{2,400}$	$IFp_{1,1}$	$IFp_{1,100}$	$IFp_{2,1}$	$IFp_{2,400}$
	%	%	%	%	%	%	%	%
Reinforced with EPS 30/20								
Peak settlement	2.44	4.36	10.97	31.05	0.77	1.49	3.2	17.13
Res. Settlement	0.26	2.04	7.43	34.14				
Reinforced with EPS 20/20								
Peak settlement	1.27	2.18	5.48	15.53	-6.66	-6.29	-13.08	-8.01
Res. Settlement	0.13	1	3.75	17.09				
Reinforced with EPS 10/10								
Peak settlement	-47.54	-57.81	-127.52	Failed	-13.02	-14.42	-21.63	-93.93
Res. Settlement	-21.25	-51.92	-146.48	Failed				

** Negative values indicate insufficiency of underlying EPS geofoam despite geocell reinforcement*

Table 6.

Improvement factors of reinforced soil with thicknesses 400, 500 and 600 mm compared to unreinforced 600 mm soil thickness on EPS 20/20

Type of settlement	IFδ (reinforced compared with unreinforced case)				IFp (reinforced compared with unreinforced case)			
	First loading stage (Pm = 275 kPa)		Second loading stage (Pm =550 kPa)		First loading stage (Pm = 275 kPa)		Second loading stage (Pm =550 kPa)	
	$IF\delta_{1,1}$	$IF\delta_{1,100}$	$IF\delta_{2,1}$	$IF\delta_{2,400}$	$IFp_{1,1}$	$IFp_{1,100}$	$IFp_{2,1}$	$IFp_{2,400}$
	%	%	%	%	%	%	%	%
hs = 600 mm								
Peak	28.54	28.73	35.2	56.39	7.03	9.95	21.64	43.61
Permanent	25.16	26.36	28.82	59.8				
hs = 500 mm								
Peak	15.71	16.08	29.19	46.06	4.25	6.49	16.89	34.1
Permanent	19.14	17.82	29.43	48.76				
hs = 400 mm								
Peak	-20.32	-23.97	3.85	19.59	-8.37	-7.31	-6.81	19.51
Permanent	4.82	-12.94	4.95	20.27				

** Negative values indicate insufficiency of underlying EPS geofoam despite geocell reinforcement*

Table 7.

Material properties values used in Finite element analysis

	Material	Soil	EPS 30	EPS 20	Geocell
Basic properties	Density (kg/m^3)	1870 ~ 1960	30	20	500
	Young's modulus (MPa)	35	9	5	200
	Poisson's ratio	0.3	0.01	0.01	0.35
Plastic properties	Angle of friction	50	5	5	-
	Dilation angle	10	1	1	-
	Flow stress ratio	0.8	0.8	0.8	-